Everything your advisor

didn't teach you about giving talks

Visuals

Renée Hlozek
hlozek@dunlap.utoronto.ca
AB 222

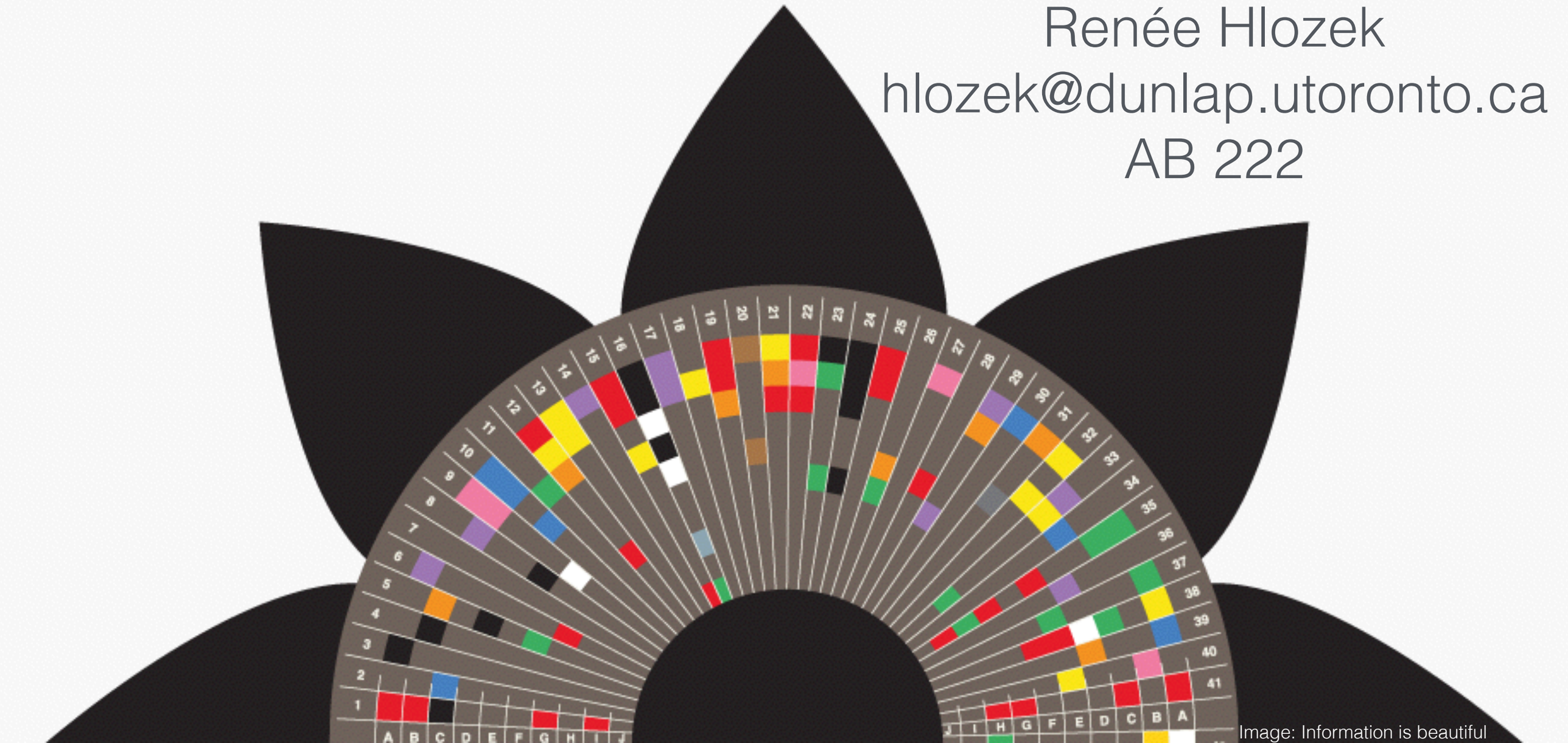

Image: Information is beautiful

Learning from the best/worst*

Data

Relationships

Dimensions

Structure

*much of what I'll teach is what I've learned from people like Alyssa Goodman

Higher dimensional/multivariate data can be tricky

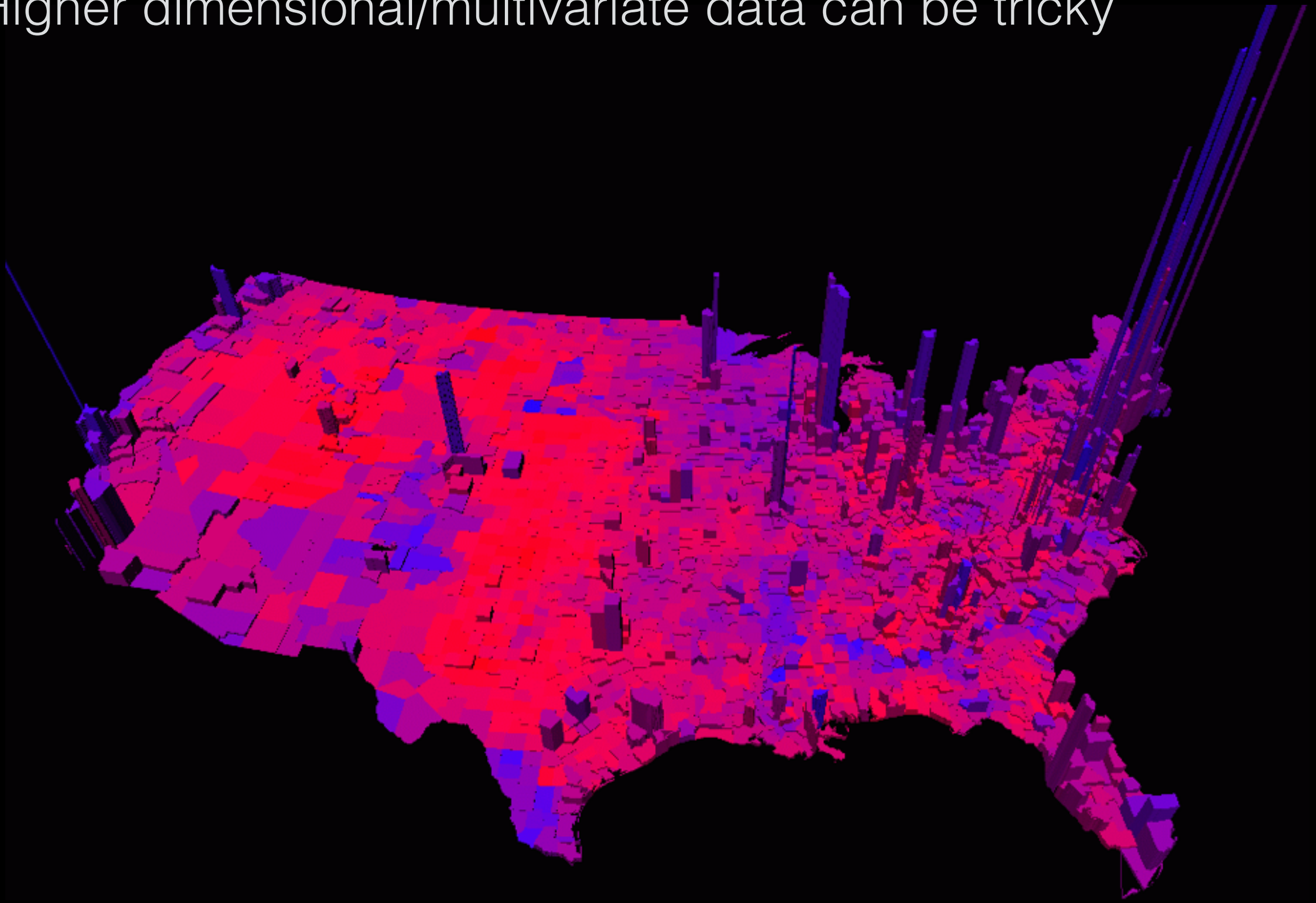

Slide from Alyssa Goodman

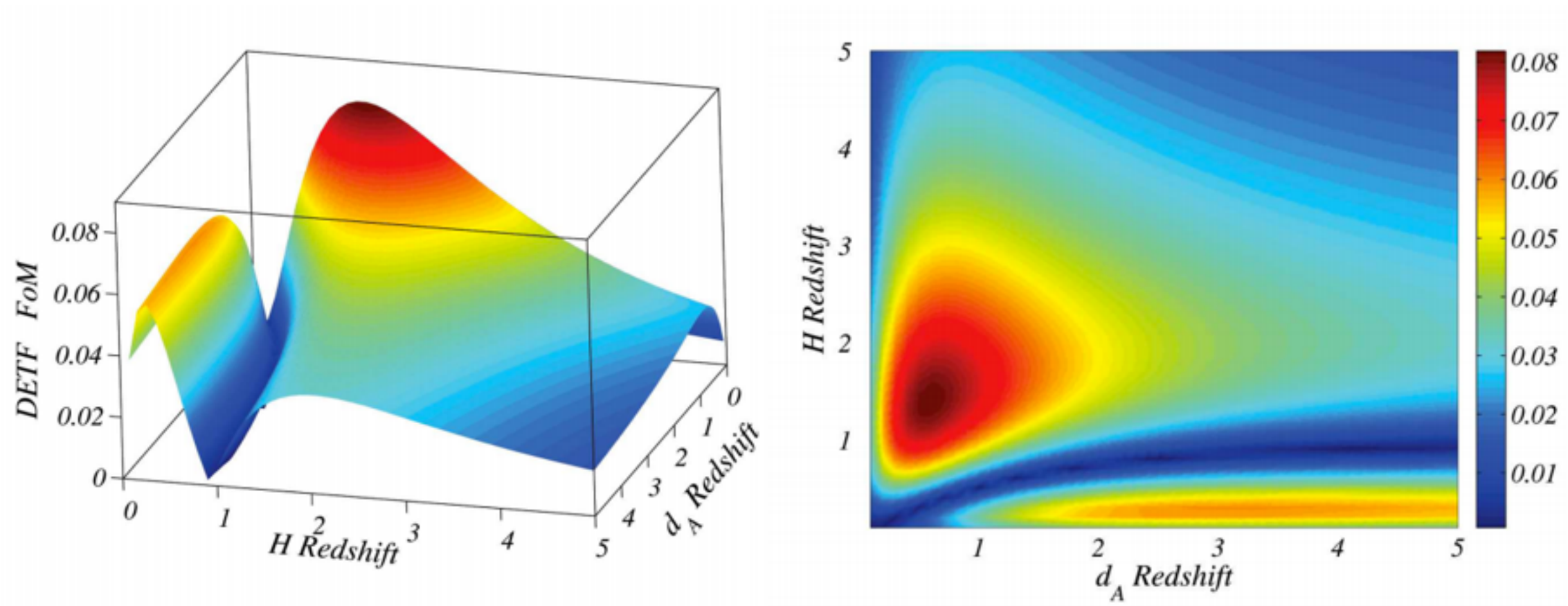

Bassett et al. 2009

Much worse for other fields like biology!

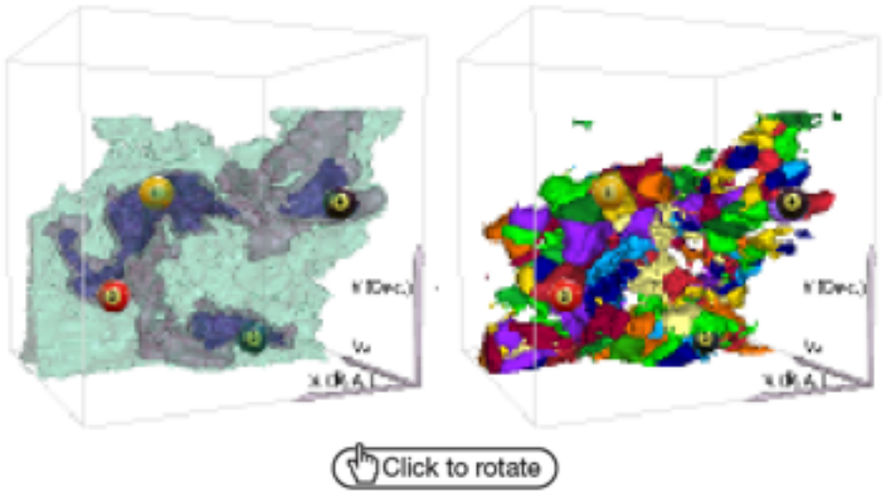

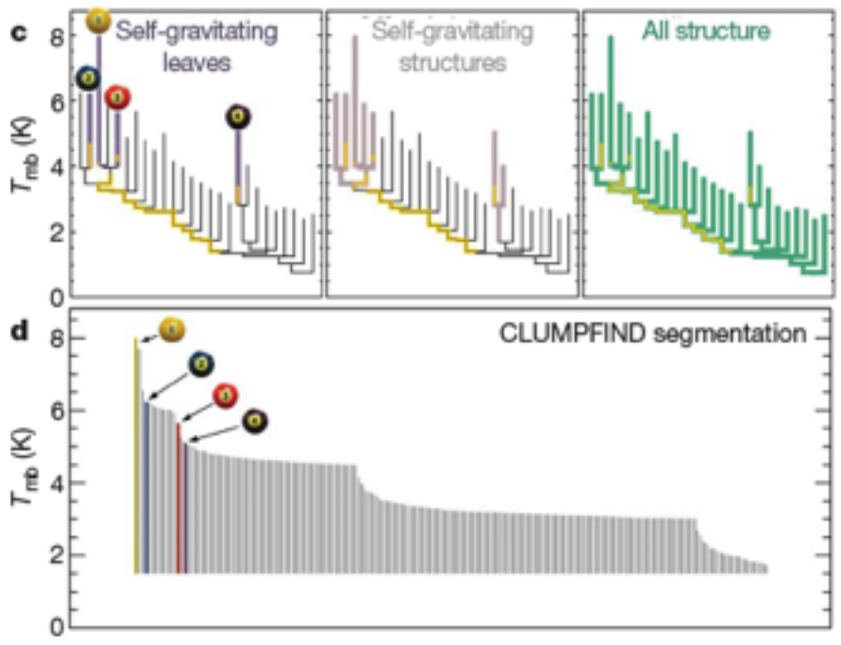

LETTERS

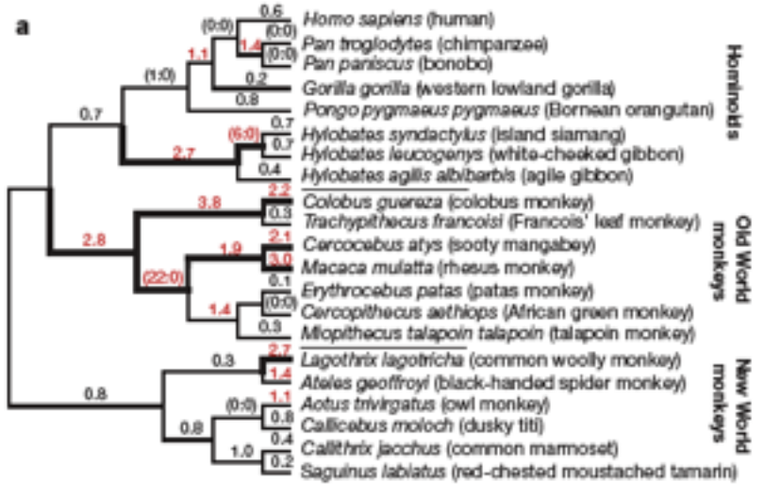

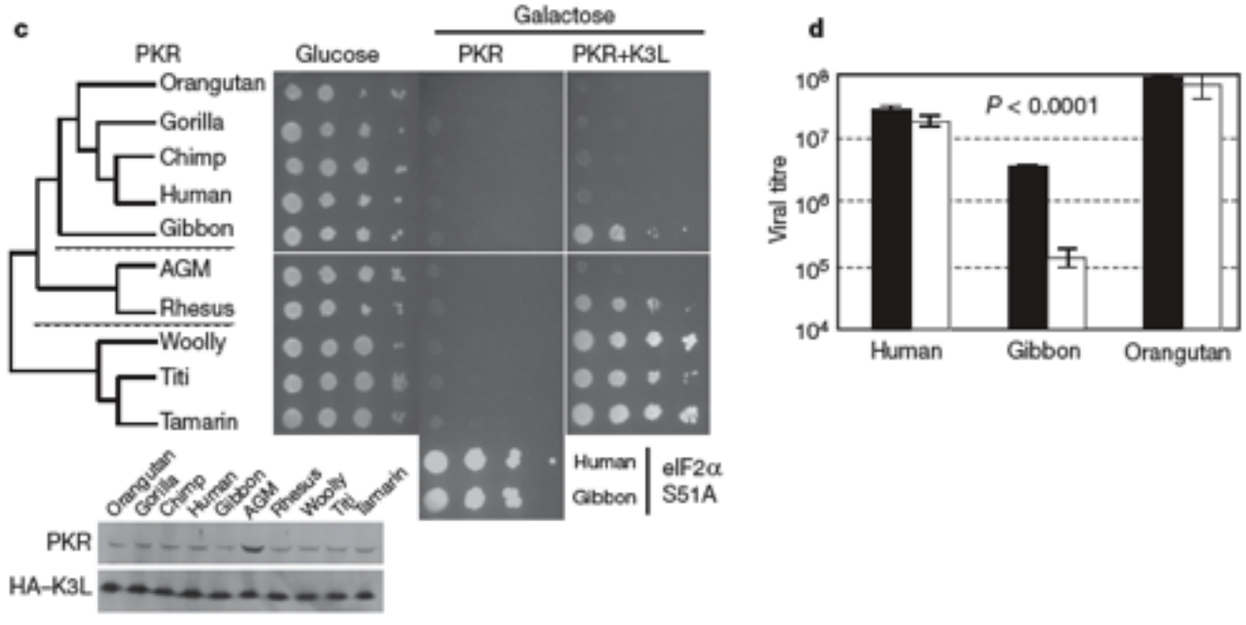

Slide from Alyssa Goodman

History of visual information

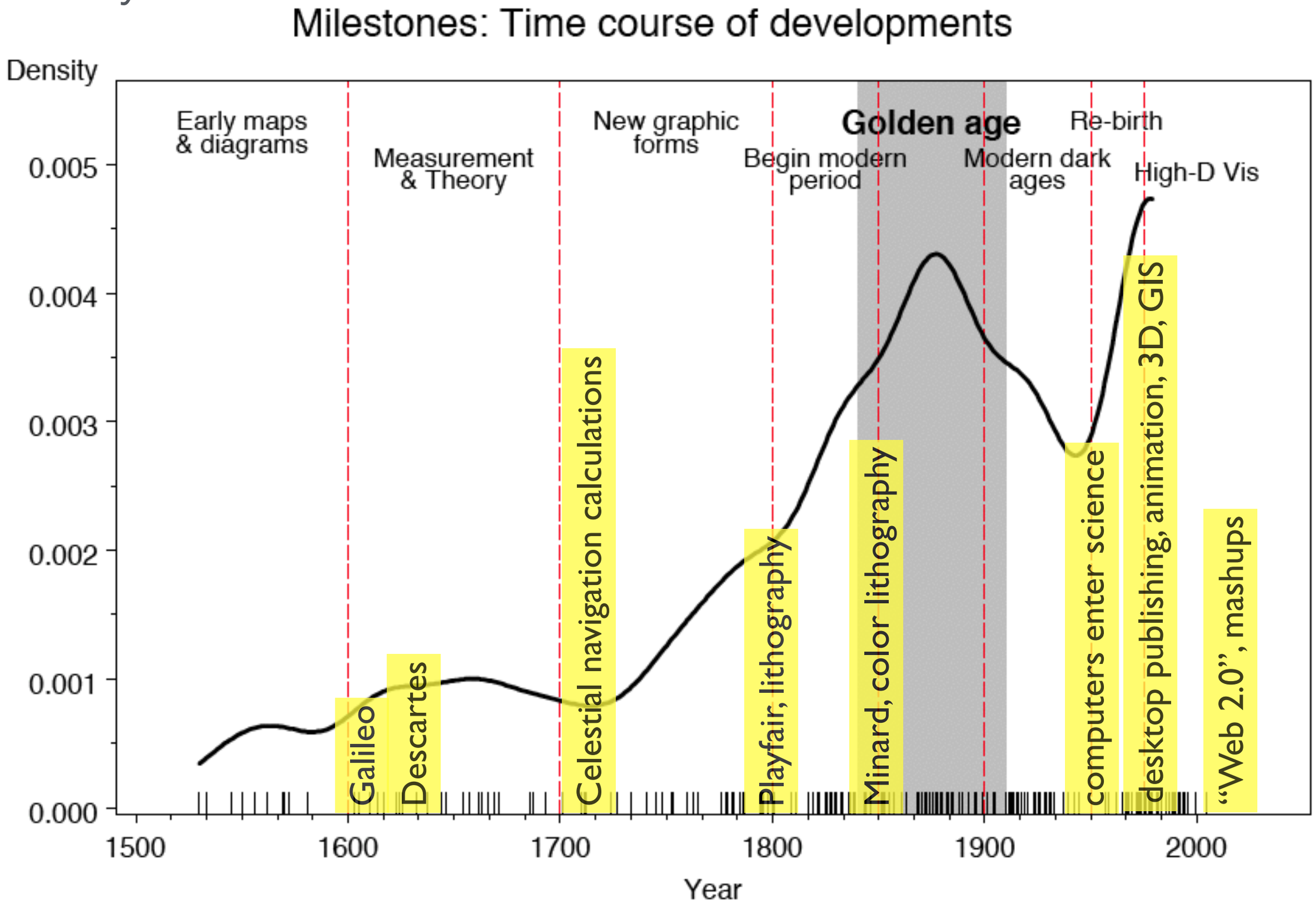

adapted from Friendly, "The Golden Age of Statistical Graphics," *Statistical Science*, 2009

Adapted from Alyssa Goodman

Galileo Galilei

(1564-1642)

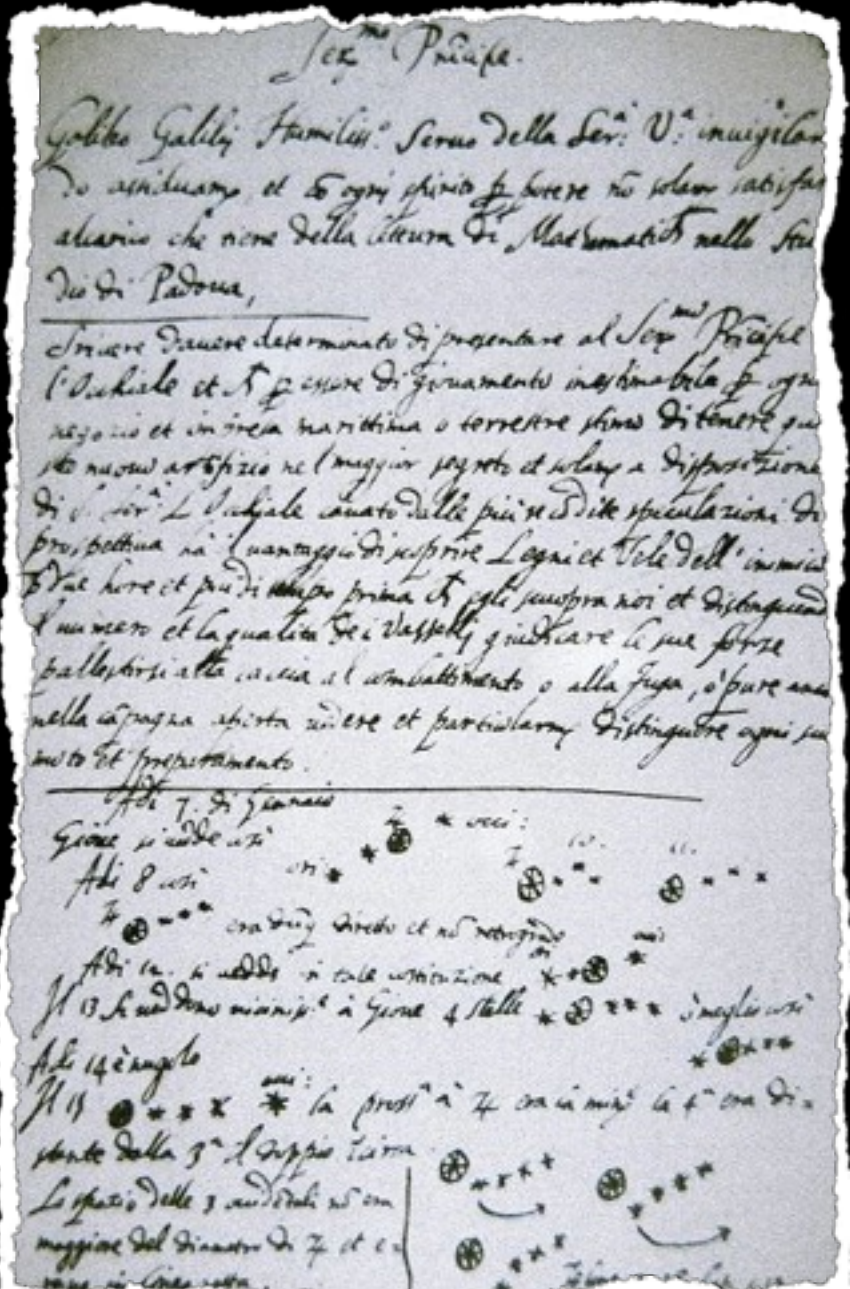

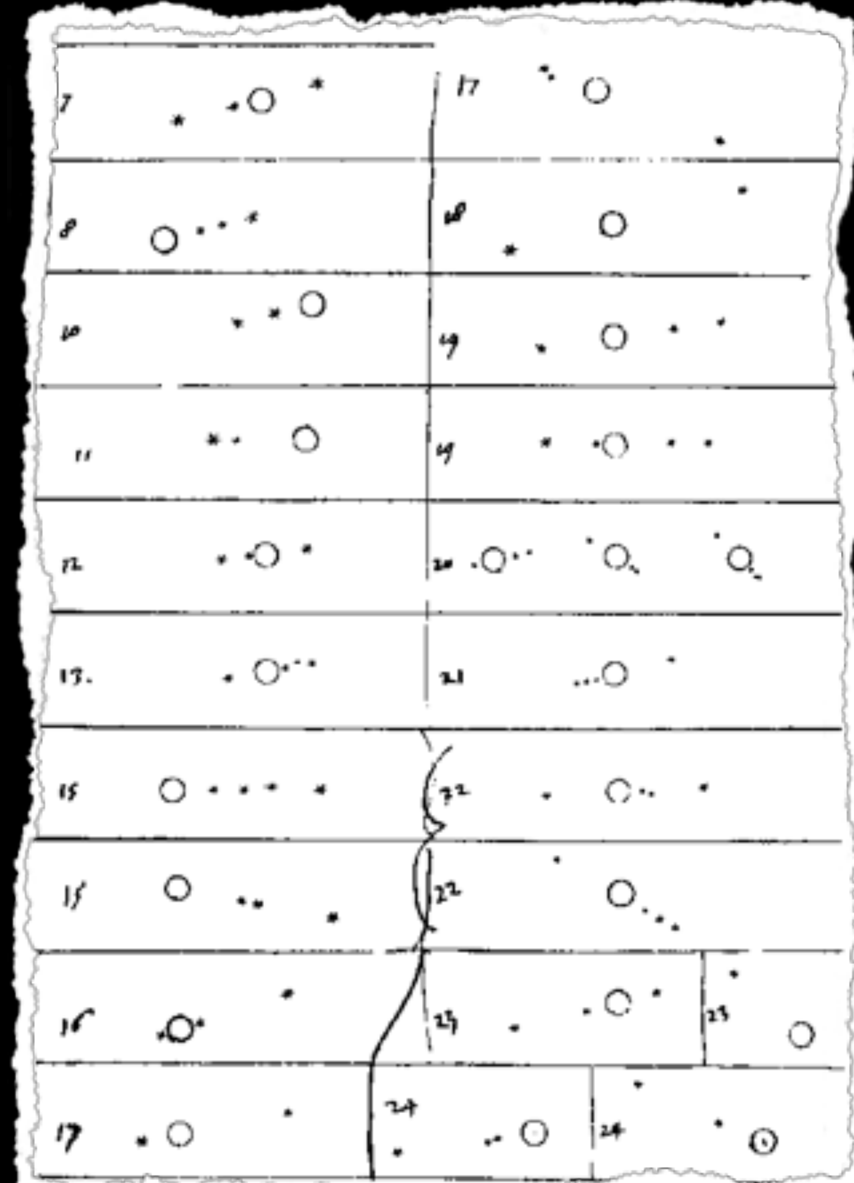

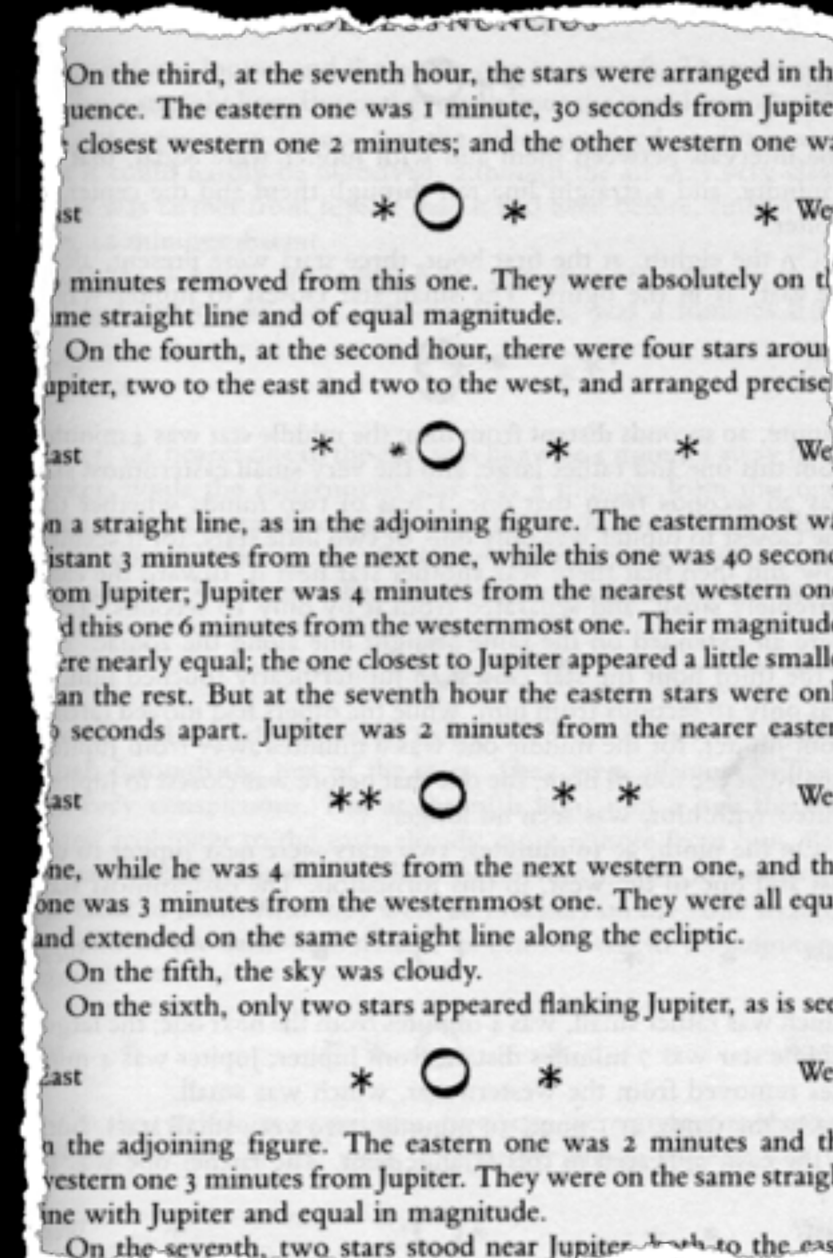

On the third, at the seventh hour, the stars were arranged in thi
quence. The eastern one was 1 minute, 30 seconds from Jupiter
closest western one 2 minutes; and the other western one wa

ast * O * * We

minutes removed from this one. They were absolutely on th
me straight line and of equal magnitude.
On the fourth, at the second hour, there were four stars arou
upiter, two to the east and two to the west, and arranged precise

ast * *O * * We

n a straight line, as in the adjoining figure. The easternmost w
istant 3 minutes from the next one, while this one was 40 second
om Jupiter; Jupiter was 4 minutes from the nearest western one
d this one 6 minutes from the westernmost one. Their magnitude
ere nearly equal; the one closest to Jupiter appeared a little smalle
an the rest. But at the seventh hour the eastern stars were only
seconds apart. Jupiter was 2 minutes from the nearer easter

ast ** O * * Wes

ne, while he was 4 minutes from the next western one, and thi
one was 3 minutes from the westernmost one. They were all equal
and extended on the same straight line along the ecliptic.
On the fifth, the sky was cloudy.
On the sixth, only two stars appeared flanking Jupiter, as is seen

ast * O * Wes

n the adjoining figure. The eastern one was 2 minutes and th
estern one 3 minutes from Jupiter. They were on the same straigh
ine with Jupiter and equal in magnitude.
On the seventh, two stars stood near Jupiter

Slide from Alyssa Goodman

Notes for & re-productions of *Siderius Nuncius* From Tufte's *Visual Display of Quantitative Information*

William Playfair
(1759-1823)

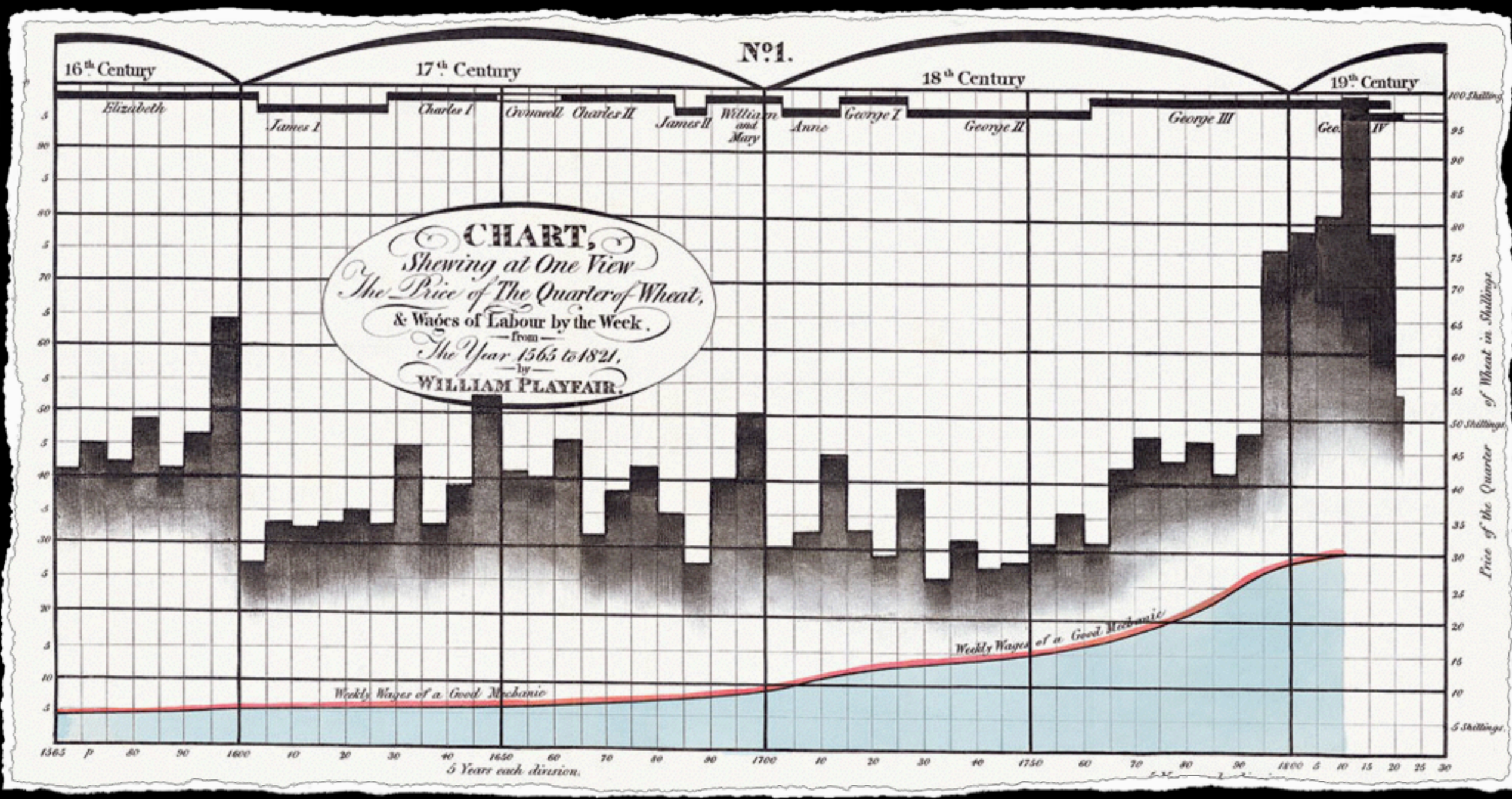

Slide from Alyssa Goodman

From Tufte's *Visual Display of Quantitative Information*

Charles Joseph Minard, in color
(1781-1870)

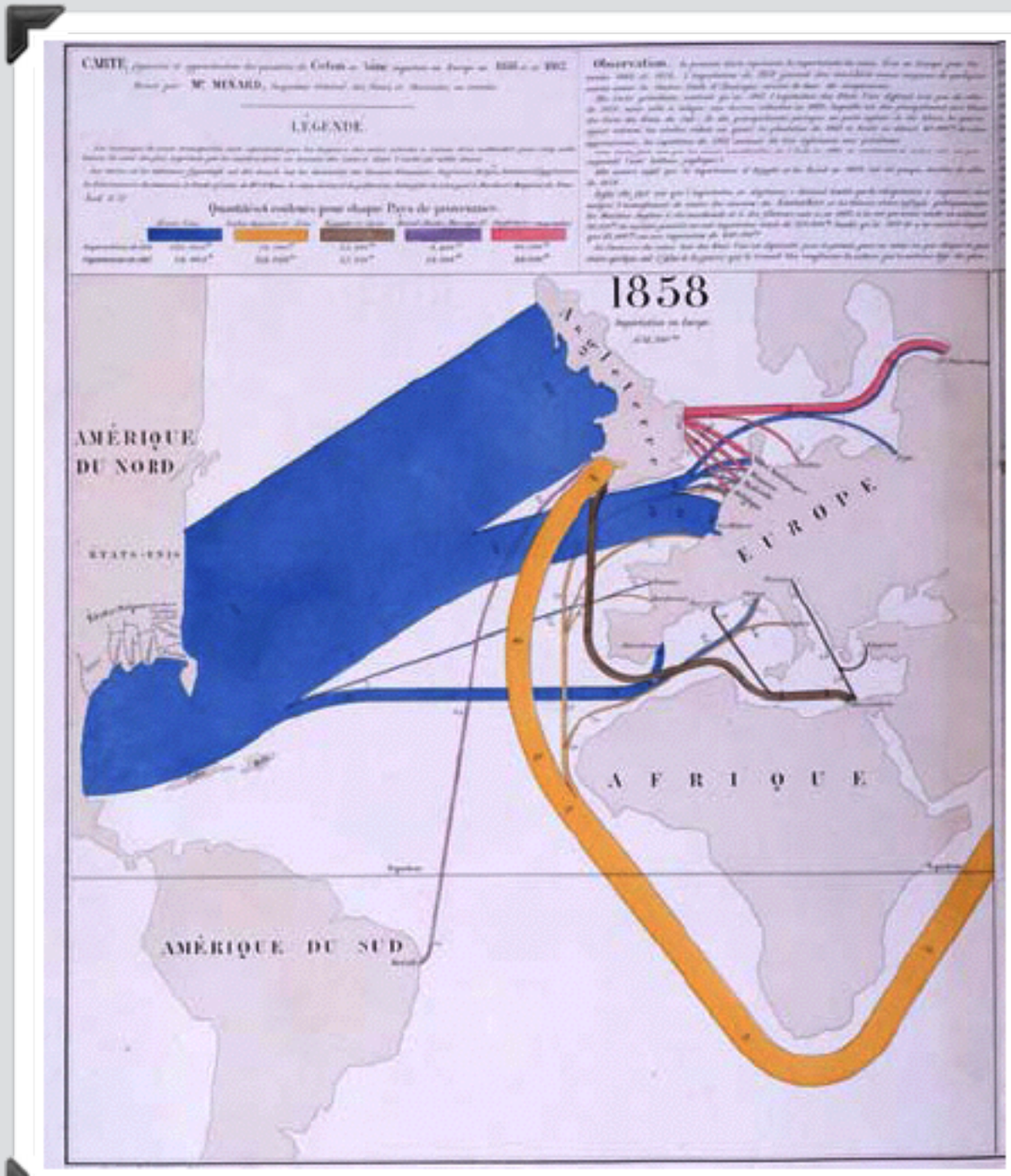

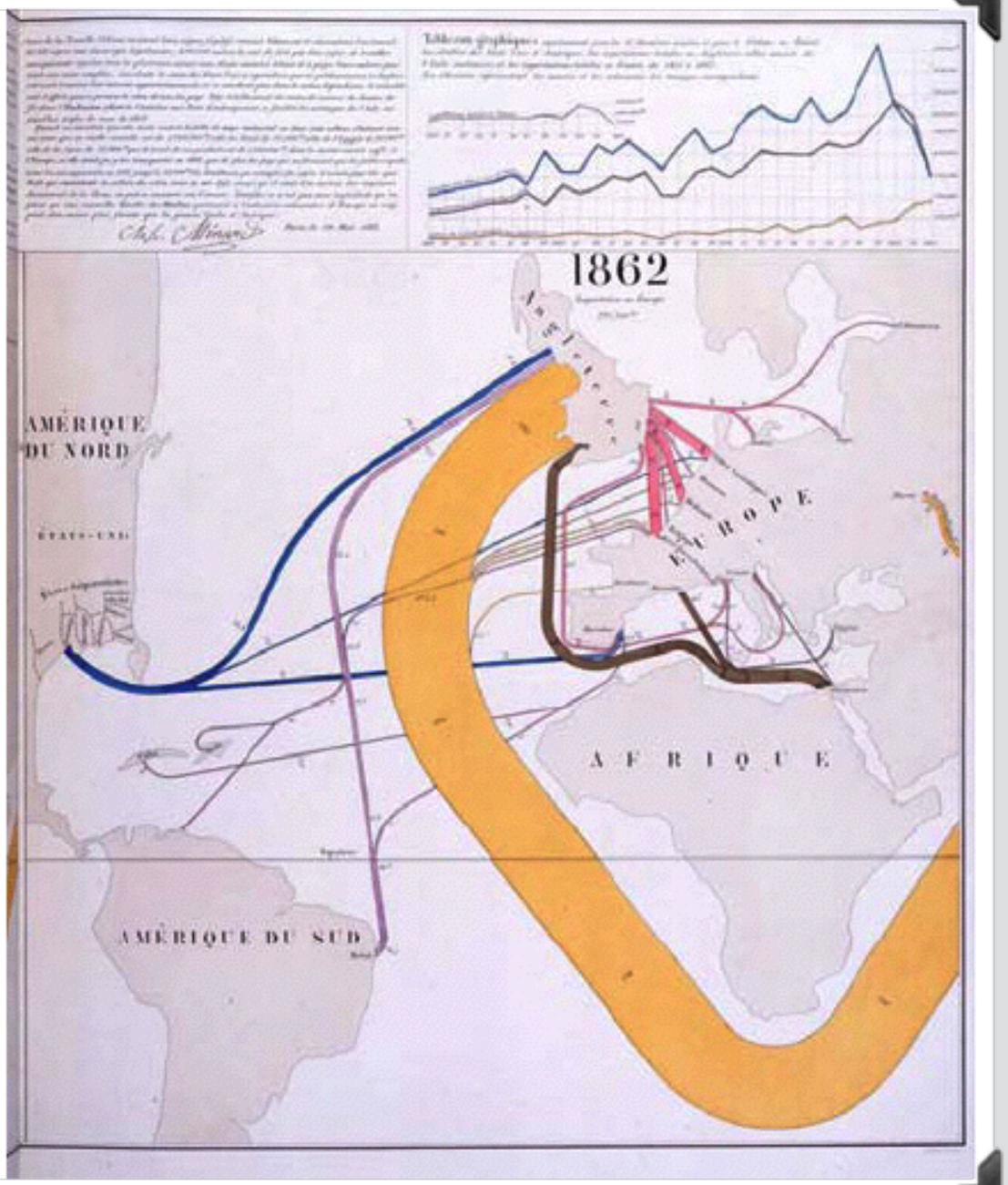

Slide from Alyssa Goodman

From Tufte's *Visual Display of Quantitative Information*

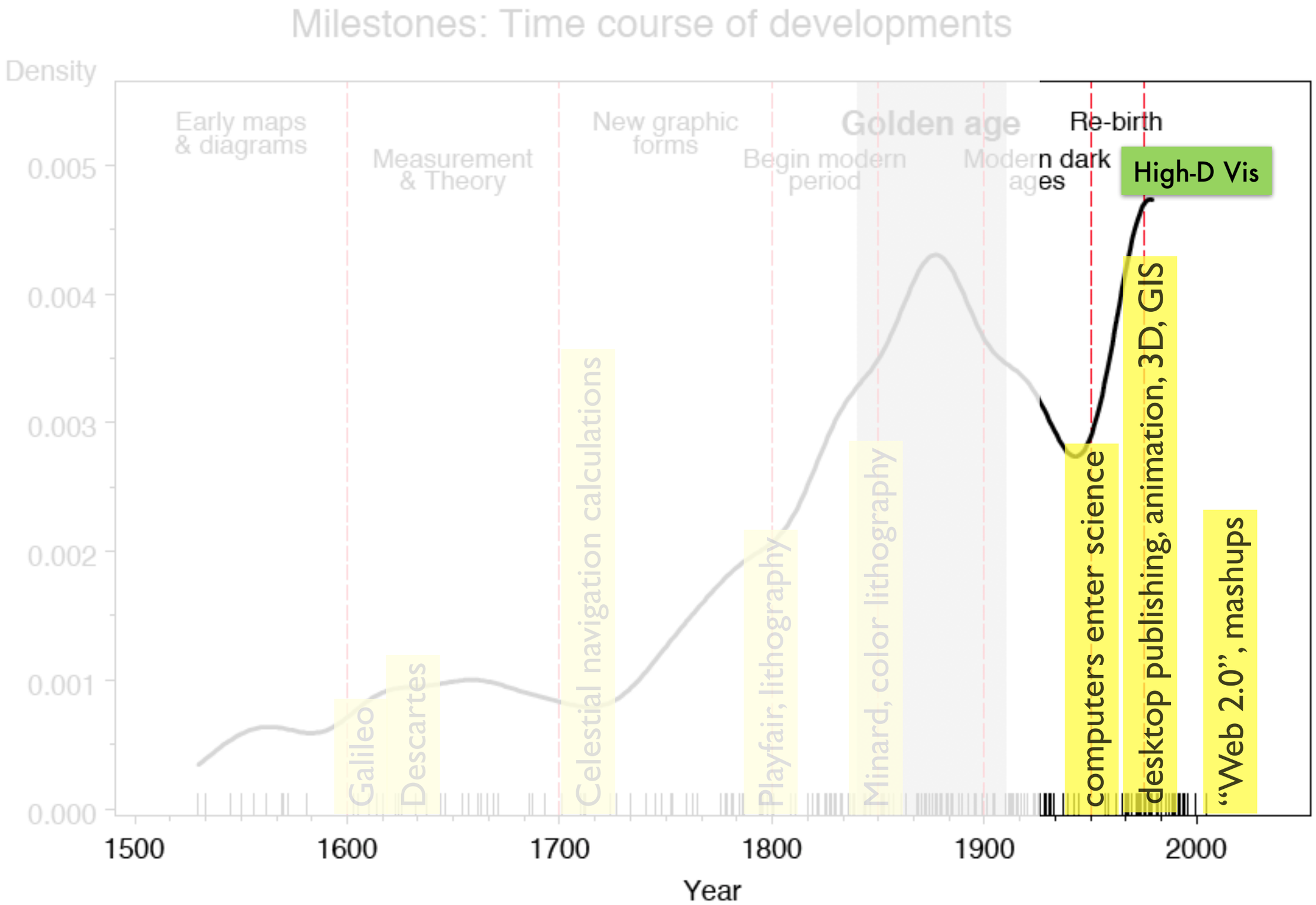

adapted from Friendly, "The Golden Age of Statistical Graphics," *Statistical Science*, 2009

Adapted from Alyssa Goodman

Interactive/3D

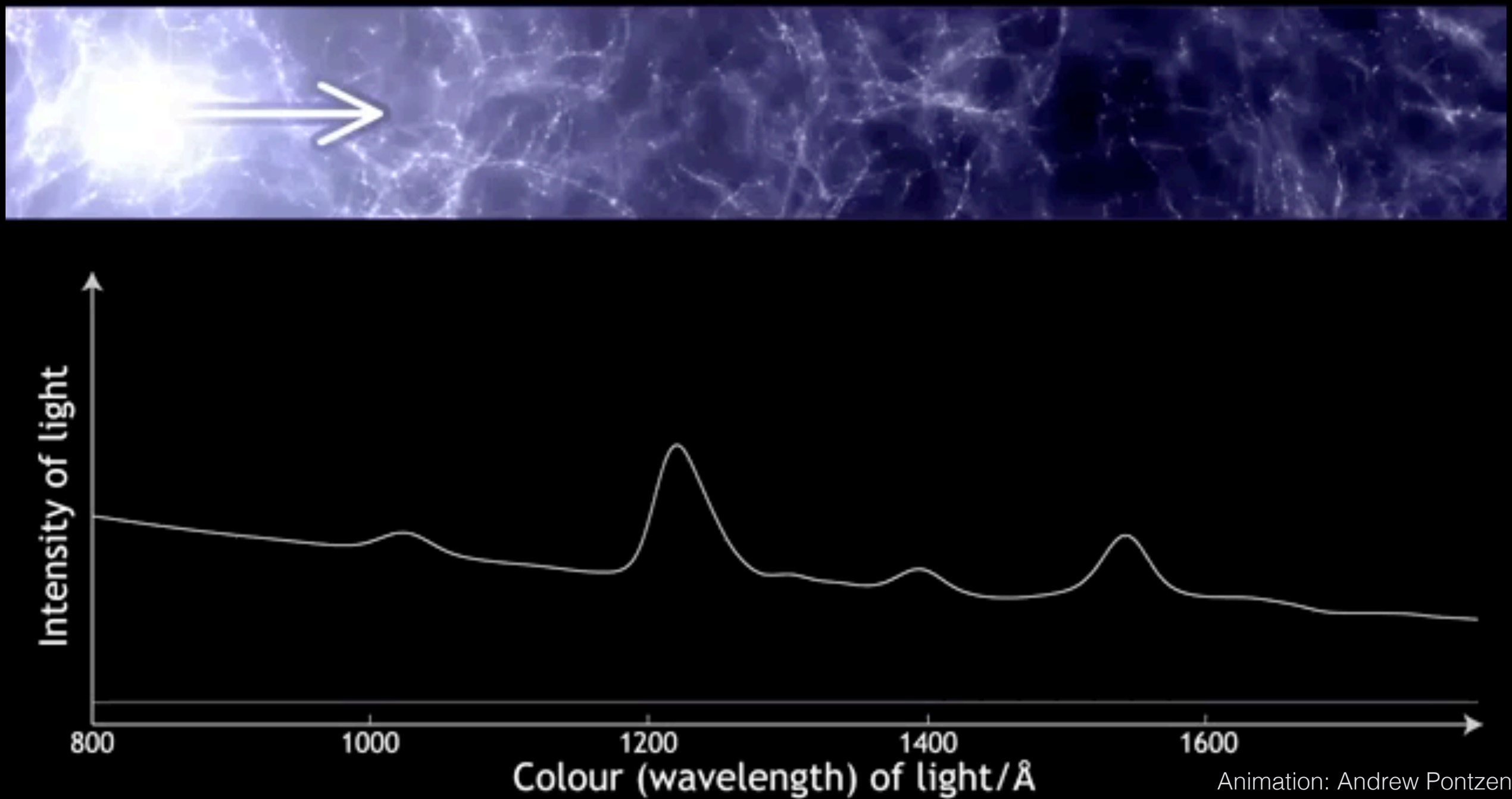

Animation: Andrew Pontzen

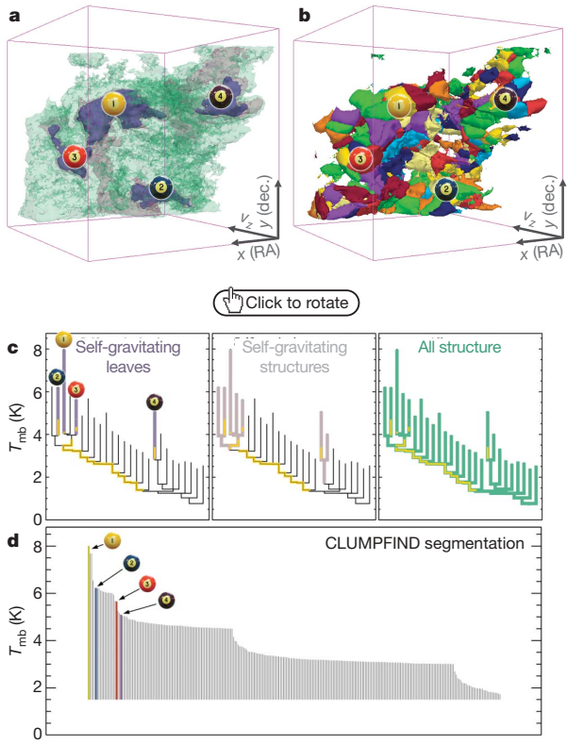

Figure 2 | Comparison of the 'dendrogram' and 'CLUMPFIND' feature-identification algorithms as applied to ^{13}CO emission from the L1448 region of Perseus. a, 3D visualization of the surfaces indicated by colours in the dendrogram shown in **c**. Purple illustrates the smallest scale self-gravitating structures in the region corresponding to the leaves of the dendrogram; pink shows the smallest surfaces that contain distinct self-gravitating leaves within them; and green corresponds to the surface in the data cube containing all the significant emission. Dendrogram branches corresponding to self-gravitating objects have been highlighted in yellow over the range of T_{mb} (main-beam temperature) test-level values for which the virial parameter is less than 2. The x–y locations of the four 'self-gravitating' leaves labelled with billiard balls are the same as those shown in Fig. 1. The 3D visualizations show position–position–velocity (p–p–v) space. RA, right ascension; dec., declination. For comparison with the ability of dendrograms (**c**) to track hierarchical structure, **d** shows a pseudo-dendrogram of the CLUMPFIND segmentation (**b**), with the same four labels used in Fig. 1 and in **a**. As 'clumps' are not allowed to belong to larger structures, each pseudo-branch in **d** is simply a series of lines connecting the maximum emission value in each clump to the threshold value. A very large number of clumps appears in **b** because of the sensitivity of CLUMPFIND to noise and small-scale structure in the data. In the online PDF version, the 3D cubes (**a** and **b**) can be rotated to any orientation, and surfaces can be turned on and off (interaction requires Adobe Acrobat version 7.0.8 or higher). In the printed version, the front face of each 3D cube (the 'home' view in the interactive online version) corresponds exactly to the patch of sky shown in Fig. 1, and velocity with respect to the Local Standard of Rest increases from front ($-0.5\,\mathrm{km\,s^{-1}}$) to back ($8\,\mathrm{km\,s^{-1}}$).

data, CLUMPFIND typically finds features on a limited range of scales, above but close to the physical resolution of the data, and its results can be overly dependent on input parameters. By tuning CLUMPFIND's two free parameters, the same molecular-line data set[8] can be used to show either that the frequency distribution of clump mass is the same as the initial mass function of stars or that it follows the much shallower mass function associated with large-scale molecular clouds (Supplementary Fig. 1).

Four years before the advent of CLUMPFIND, 'structure trees'[9] were proposed as a way to characterize clouds' hierarchical structure using 2D maps of column density. With this early 2D work as inspiration, we have developed a structure-identif… …lgorithm that abstracts the hierarchical structure of a 3D… an easily visualized representation called a '… well developed in other data-intensive field… application of tree methodologies so far in … and almost exclusively within the area … 'merger trees' are being used with increa…

Figure 3 and its legend explain the co… schematically. The dendrogram quantifi… ima of emission merge with each othe… explained in Supplementary Methods. … determined almost entirely by the da… sensitivity to algorithm parameters. T… possible on paper and 2D screens, we… data (see Fig. 3 and its legend), by… cross, which eliminates dimensiona… preserving all information abo… Numbered 'billiard ball' labels i… features between a 2D map (Fig. … online) and a sorted dendrogra…

A dendrogram of a spectral-li… of key physical properties associ… surfaces, such as radius (R), velocity dispers… (L). The volumes can have any shape, and in other work … the significance of the especially elongated features seen in L1448 (Fig. 2a). The luminosity is an approximate proxy for mass, such that $M_{\mathrm{lum}} = X_{13\mathrm{CO}} L_{13\mathrm{CO}}$, where $X_{13\mathrm{CO}} = 8.0 \times 10^{20}\,\mathrm{cm^2\,K^{-1}\,km^{-1}\,s}$ (ref. 15; see Supplementary Methods and Supplementary Fig. 2). The derived values for size, mass and velocity dispersion can then be used to estimate the role of self-gravity at each point in the hierarchy, via calculation of an 'observed' virial parameter, $\alpha_{\mathrm{obs}} = 5\sigma_v^2 R/GM_{\mathrm{lum}}$. In principle, extended portions of the tree (Fig. 2, yellow highlighting) where $\alpha_{\mathrm{obs}} < 2$ (where gravitational energy is comparable to or larger than kinetic energy) correspond to regions of p–p–v space where self-gravity is significant. As α_{obs} only represents the ratio of kinetic energy to gravitational energy at one point in time, and does not explicitly capture external over-pressure and/or magnetic fields[16], its measured value should only be used as a guide to the longevity (boundedness) of any particular feature.

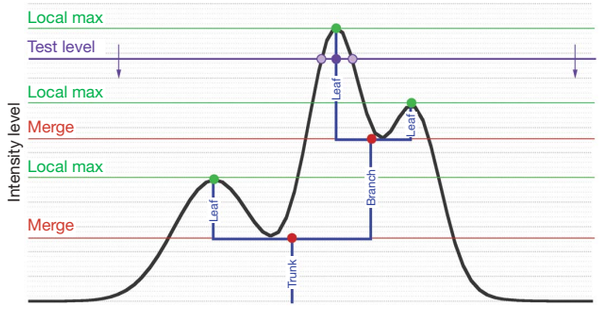

Figure 3 | Schematic illustration of the dendrogram process. Shown is the construction of a dendrogram from a hypothetical one-dimensional emission profile (black). The dendrogram (blue) can be constructed by 'dropping' a test constant emission level (purple) from above in tiny steps (exaggerated in size here, light lines) until all the local maxima and mergers are found, and connected as shown. The intersection of a test level with the emission is a set of points (for example the light purple dots) in one dimension, a planar curve in two dimensions, and an isosurface in three dimensions. The dendrogram of 3D data shown in Fig. 2c is the direct analogue of the tree shown here, only constructed from 'isosurface' rather than 'point' intersections. It has been sorted and flattened for representation on a flat page, as fully representing dendrograms for 3D data cubes would require four dimensions.

“Never Underestimate the Bivariate Scatter Plot”

-E. Rosolowsky, 2013

Slide from Alyssa Goodman

History of the AG,

http://www.astronomische-gesellschaft.org/Tagungen_eng.html

All meetings since 1863:

(RGA = regular meeting of the General Assembly)

Year	RGA	City	Date	Members	Atendees	Lectures	Poster
2009	82	Potsdam	Sep. 21-25		360 (138 members, 92 students)	185 (23 plenary talks, 162 splinter talks)	102
2008	81	Vienna (A)	Sep. 07-12	774	482		
2008		*Spring:* Strasbourg (F)	Mar. 16-20				
2007	80	Würzburg	Sep. 24-28	799			
2005	79	Cologne	Sep.26-Oct.01	803			
2004	78	Prague (CZ)	Sep. 20-25	803	178	107	67
2004		Hamburg	July 05-09				
2003	77	Freiburg	Sep. 15-20	801	250	160	110
2002	76	Berlin	Sep. 23-28	796	270	143	120
2001	75	Munich	Sep. 10-14	793	530	187	180
2000	74	Bremen	Sep. 18-23	795	235	87	110
2000		*Spring:* Nördlingen	May 16-20				
2000		Heidelberg	Mar. 20-24				
1999	73	Göttingen	Sep. 20-25	809	350	163	125
1998	72	Heidelberg	Sep. 14-19	805	380	184	155
1998		*Spring:* Gotha	May 11-15				
1997	71	Innsbruck (A)	Sep. 22-27	798	340	155	118
1996	70	Tübingen	Sep. 16-21	805	295	165	98
1995	69	Bonn	Sep. 18-23	796	400	198	116
1994	68	Potsdam	Sep. 26-30	771	430	113	145

History of the AG,

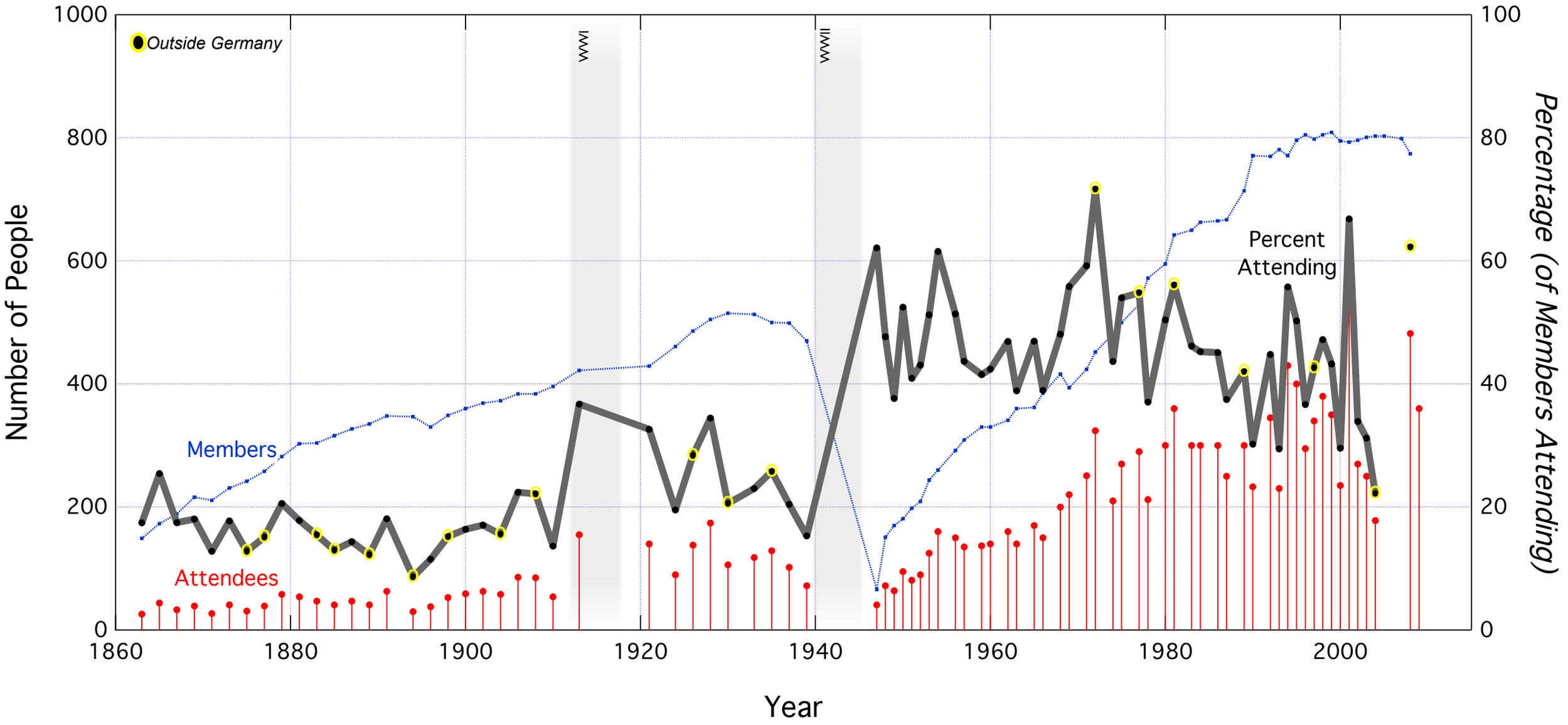

Adapted from Alyssa Goodman

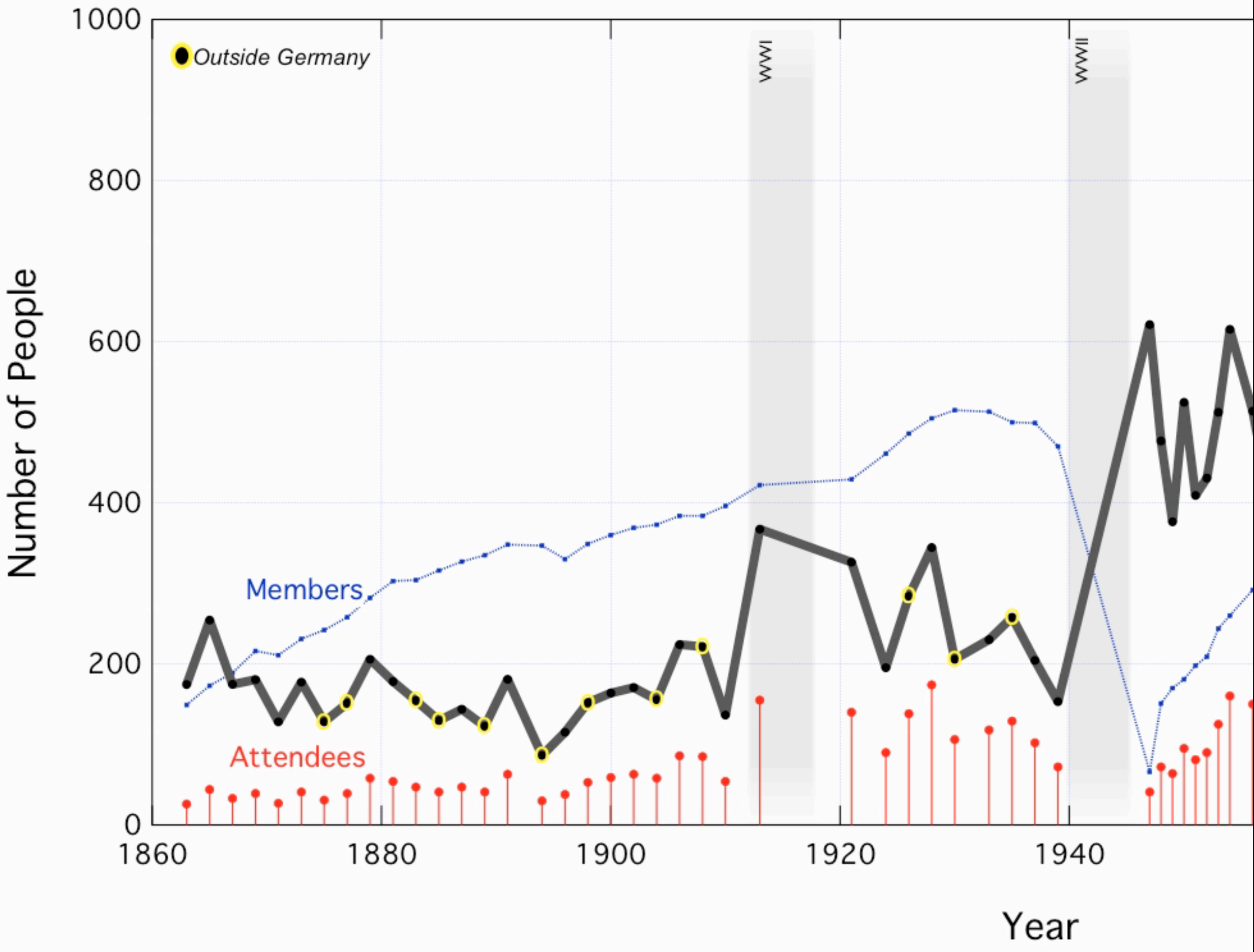
Outside Germany
WWI
WWII
Members
Attendees
Number of People
Year
1000
800
600
400
200
0
1860
1880
1900
1920
1940

Plots we love

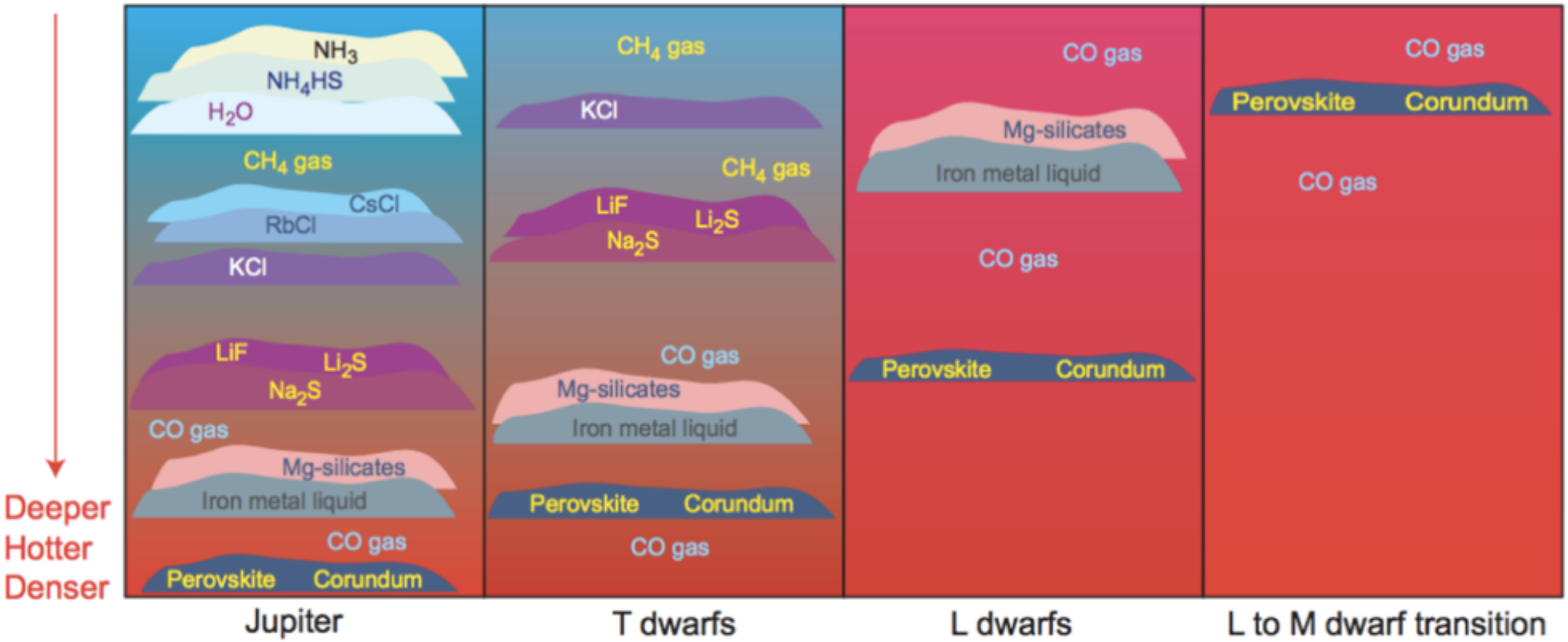

A cloudy picture. Cloud layers for Jupiter, T dwarfs, L dwarfs, and objects near the transition from L to M dwarfs. The layers are progressively stripped off as the temperature of the object increases.

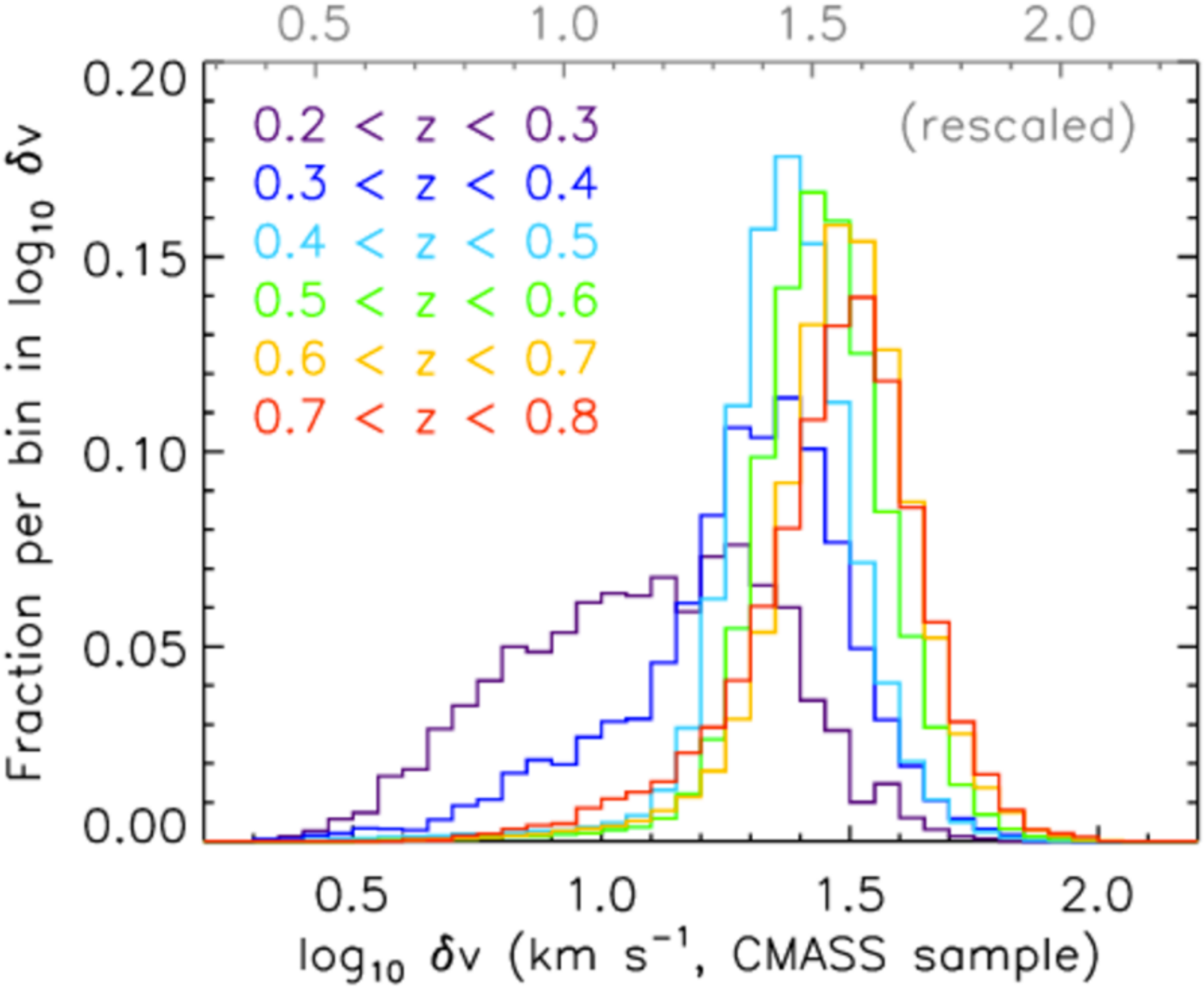
0.5
1.0
1.5
2.0
0.20
0.15
0.10
0.05
0.00
0.2 < z < 0.3
0.3 < z < 0.4
0.4 < z < 0.5
0.5 < z < 0.6
0.6 < z < 0.7
0.7 < z < 0.8
(rescaled)
Fraction per bin in log10 δv
log10 δv (km s−1, CMASS sample)

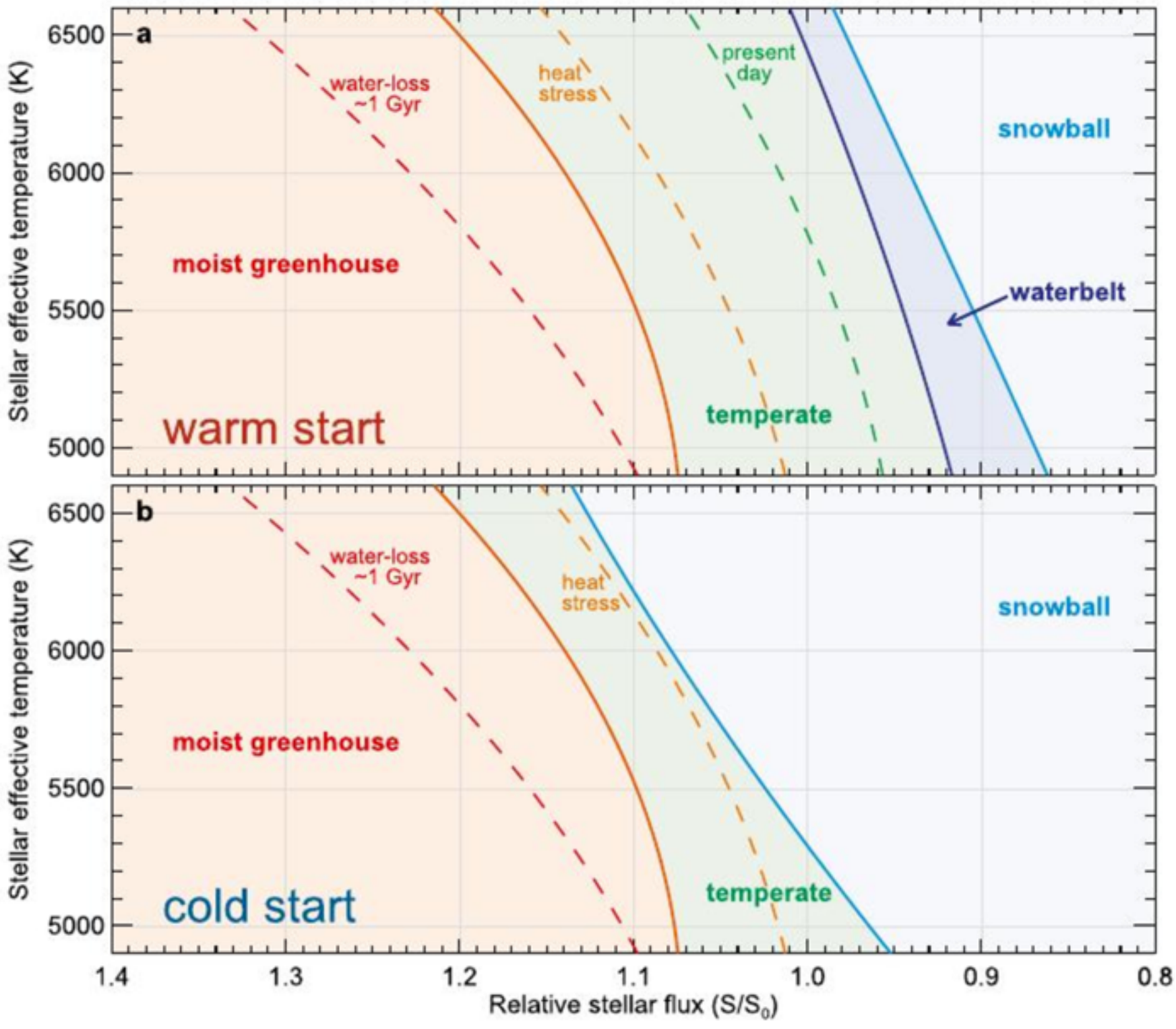

Figure 4. Circumstellar climate zones as a function of relative stellar flux for Earth-like planets at constant CO_2. The top panel assumes an initial state that is warm (i.e., liquid water covers the surface). The bottom panel assumes an initial state of a completely ice-covered planet.

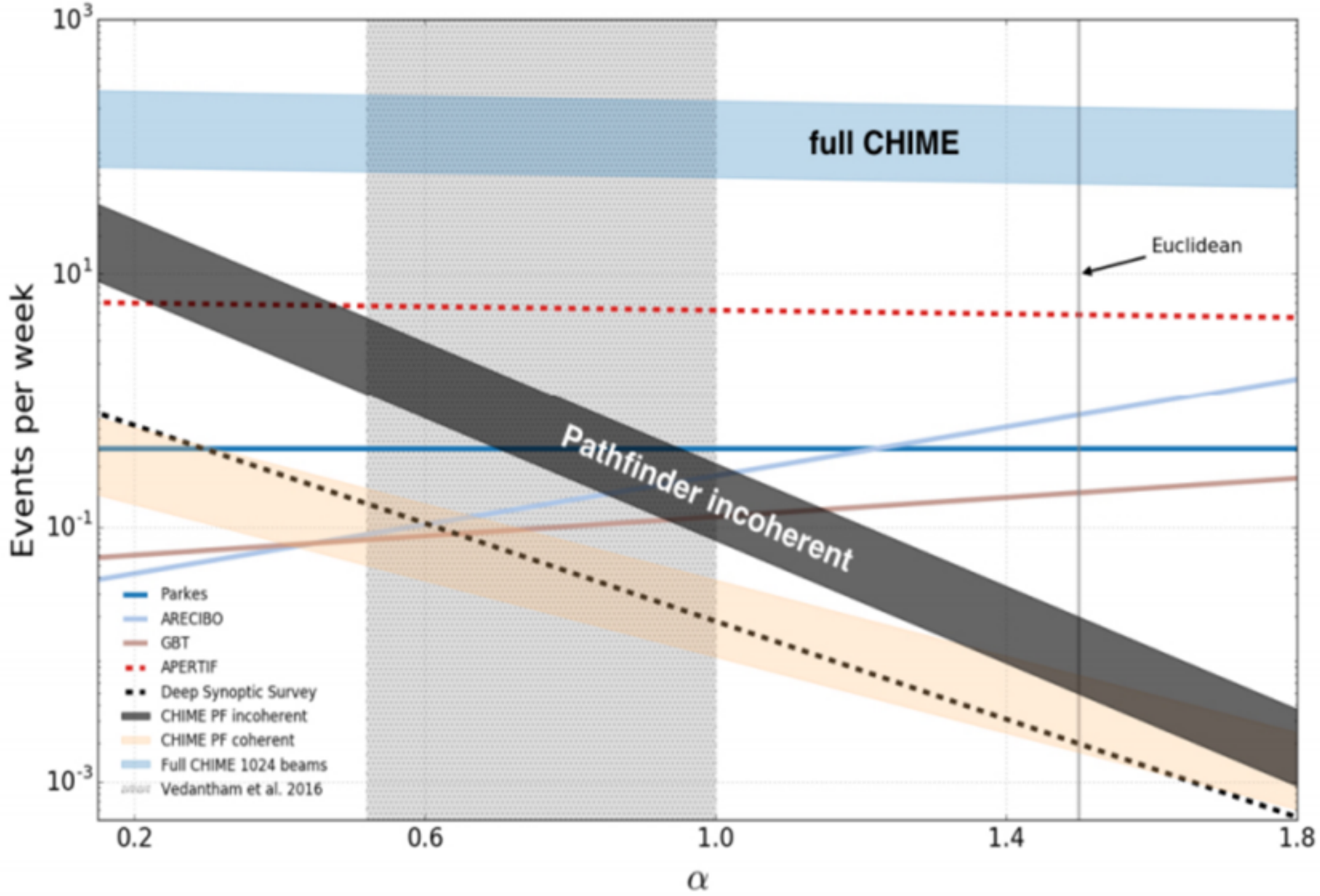

Figure 1. Weekly event rates for several different surveys plotted as a function of brightness distribution parameter α, pinned to the Parkes rate (hence its flatness), similar to what is done in Eq. 11 with GBT. The three solid lines are surveys that have already found FRBs. The light grey dotted region shows the 90% confidence interval of α proposed by Vedantham et al. (2016). The thick colored regions allow for uncertainty in the rate below 1.4 GHz, and the dashed curves are for 1.4 GHz surveys still in the commissioning phase. Interestingly, the modestly sized CHIME Pathfinder in incoherent mode (dark grey) would be the fastest survey to date in incoherent mode, if $\alpha \lesssim 0.75$. This is due to its 200 deg^2 primary beam and the importance of FoV for small α.

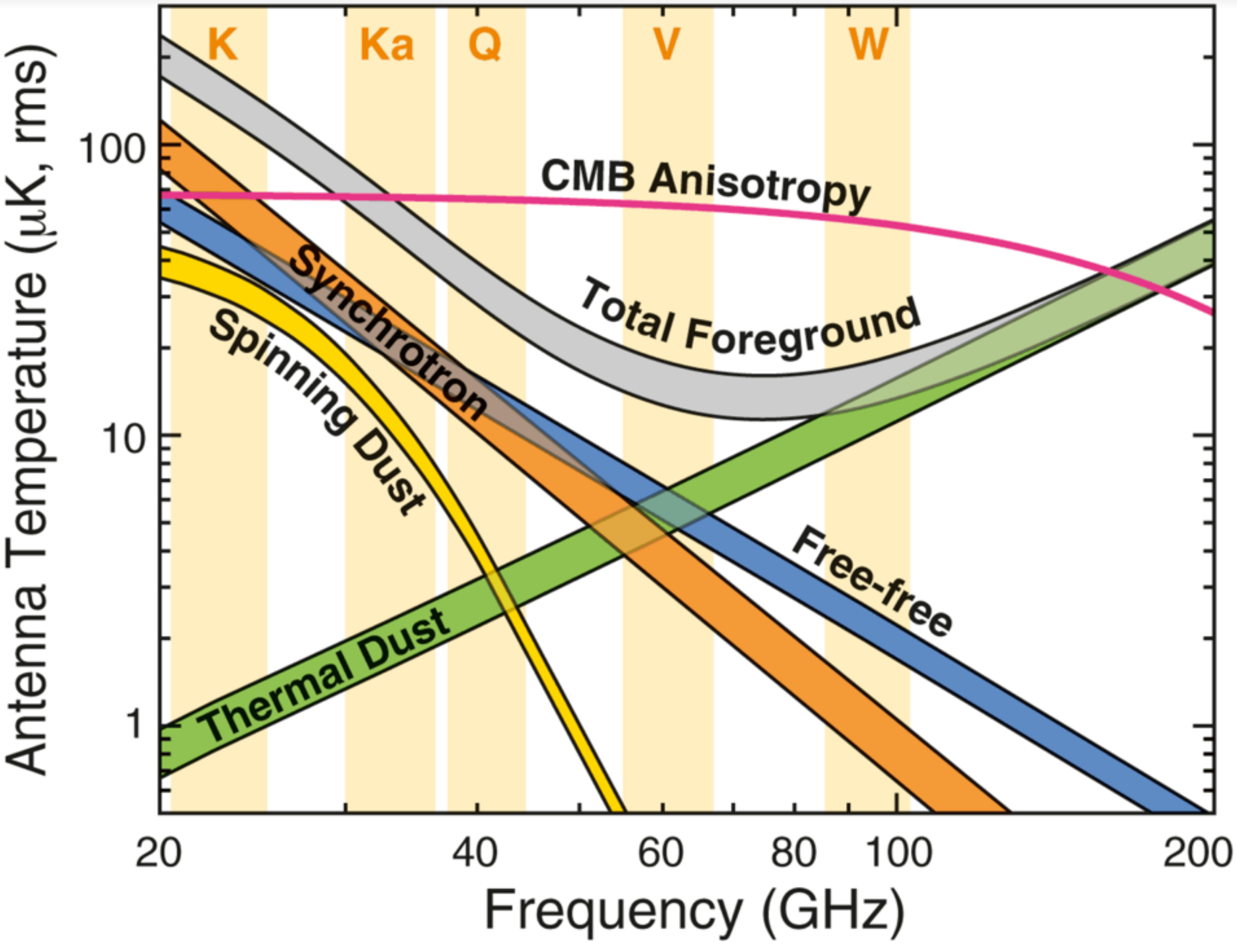
K
Ka
Q
V
W
CMB Anisotropy
Total Foreground
Synchrotron
Spinning Dust
Thermal Dust
Free-free
100
10
1
Antenna Temperature (μK, rms)
20
40
60
80
100
200
Frequency (GHz)

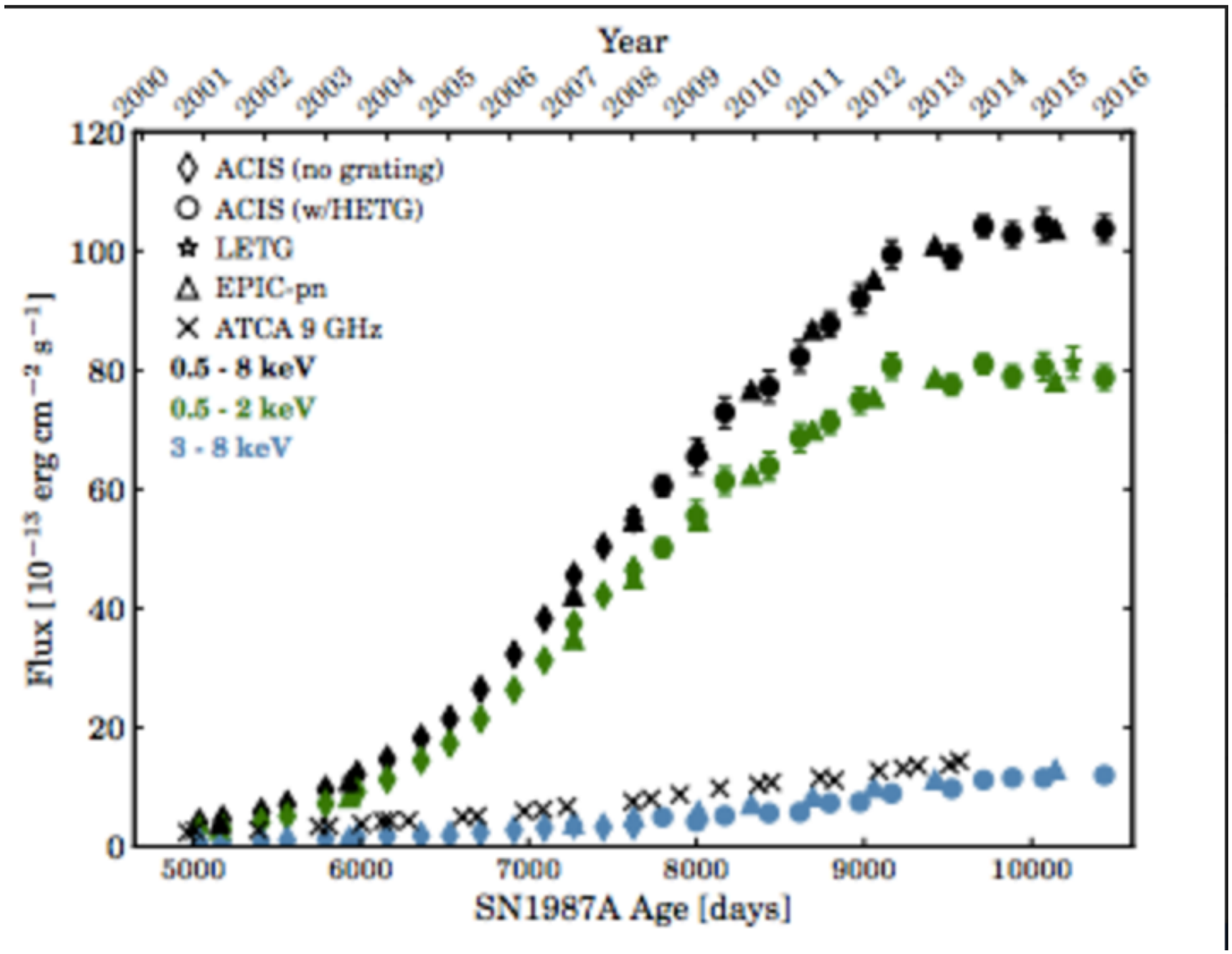
Year
2000
2001
2002
2003
2004
2005
2006
2007
2008
2009
2010
2011
2012
2013
2014
2015
2016
ACIS (no grating)
ACIS (w/HETG)
LETG
EPIC-pn
ATCA 9 GHz
0.5 - 8 keV
0.5 - 2 keV
3 - 8 keV
Flux [10^{-13} erg cm^{-2} s^{-1}]
120
100
80
60
40
20
0
5000
6000
7000
8000
9000
10000
SN1987A Age [days]

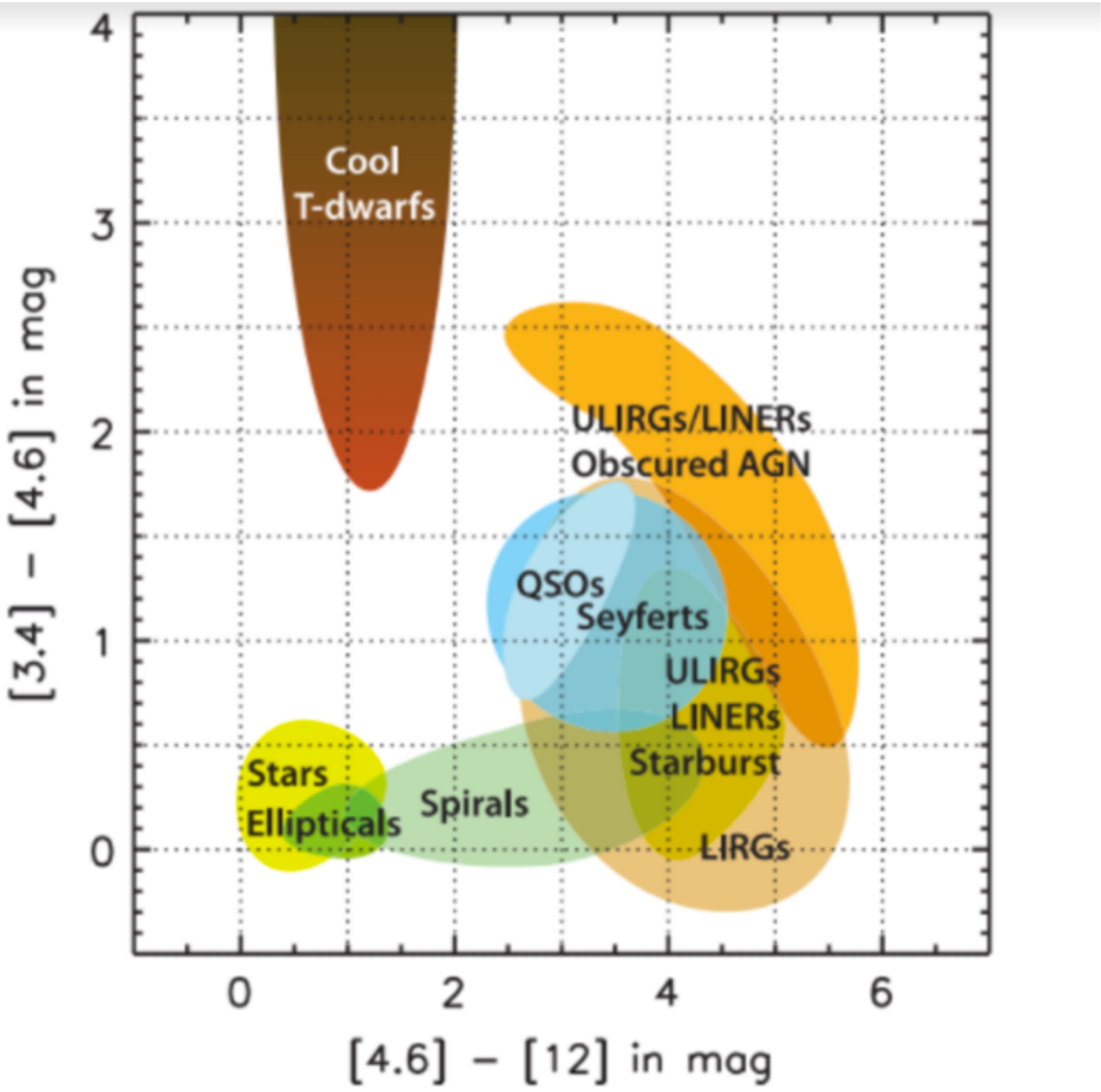

Figure 12. Color–color diagram showing the locations of interesting classes of objects. Stars and early-type galaxies have colors near zero, while brown dwarfs are very red in *W*1–*W*2, spiral galaxies are red in *W*2–*W*3, and ULIRGS tend to be red in both colors.

Plots we love

Plots we love to hate

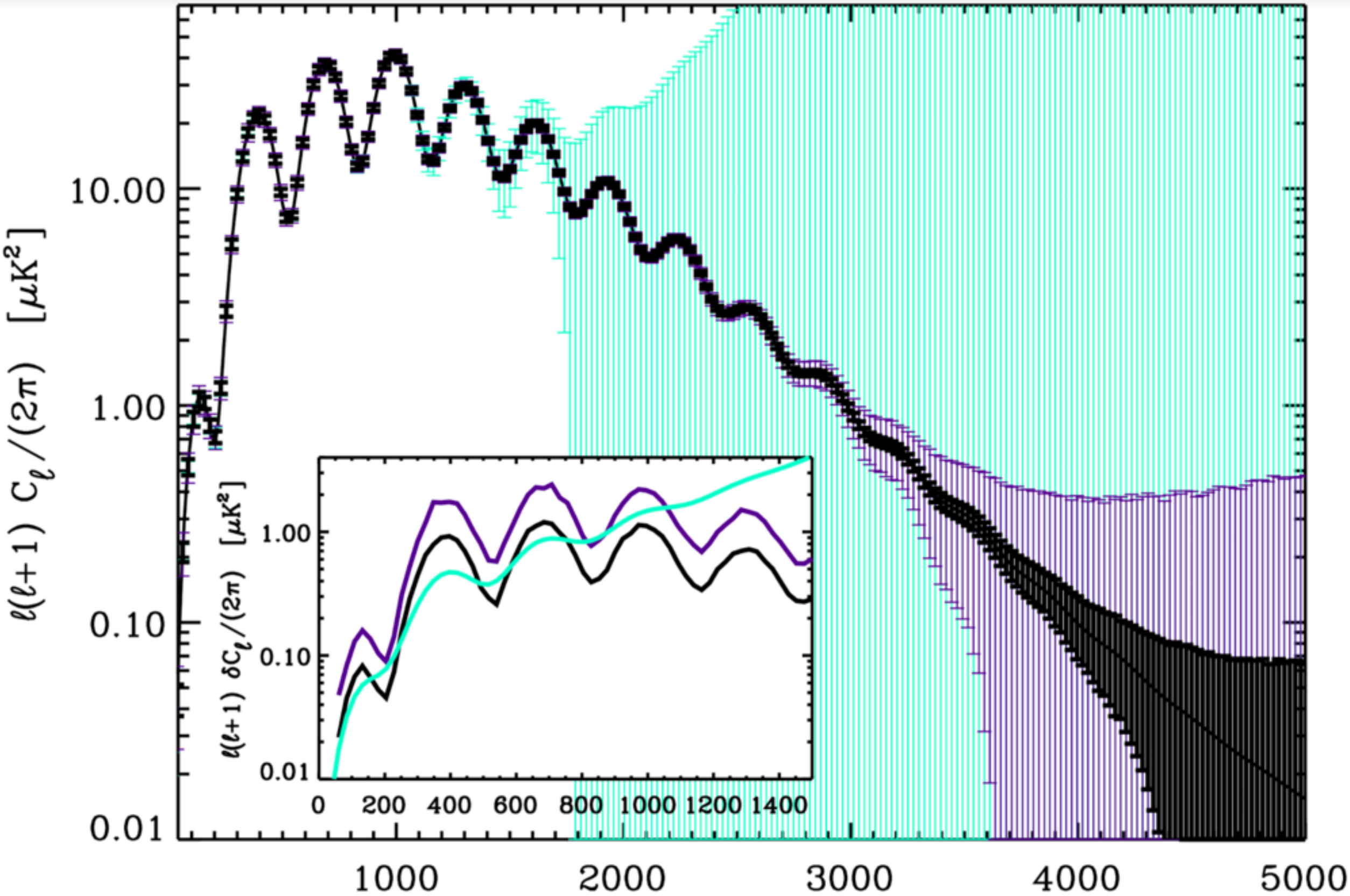
10.00
1.00
0.10
0.01
$\ell(\ell+1)\ C_\ell/(2\pi)\ \ [\mu K^2]$
1000
2000
3000
4000
5000
1.00
0.10
0.01
$\ell(\ell+1)\ \delta C_\ell/(2\pi)\ \ [\mu K^2]$
0
200
400
600
800
1000
1200
1400

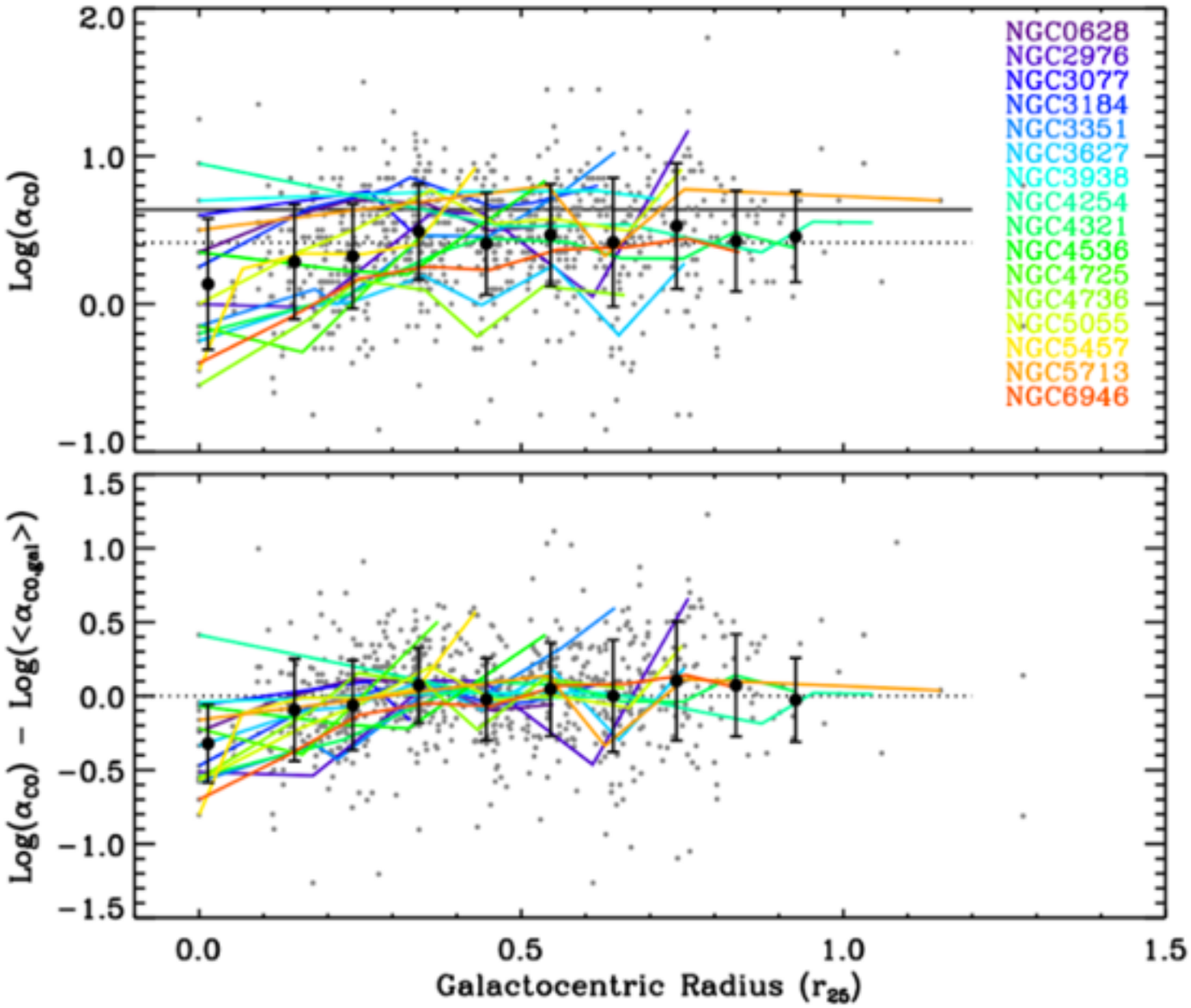

FIG. 7.— Dust-based α_{CO} determination across the disks of 22 galaxies (Sandstrom et al. 2012). The top panel shows the results for the individual regions (gray points), averages in radial bins for each galaxy (color lines), and the average trend for all data as a function of radius (black circles with error bars showing the scatter in that bin). The black solid line in the top panel corresponds to $X_{CO,20} = 2$, and the dotted line shows the average, weighting all solution pixels equally ($X_{CO,20} = 1.2$). Weighting by galaxy or CO intensity rather than line of sight, the mean is $X_{CO,20} \approx 1.4 - 1.8$ for low inclination galaxies. The bottom panel shows each galaxy normalized by its mean X_{CO} to highlight the fact that many galaxies exhibit low X_{CO} in their centers.

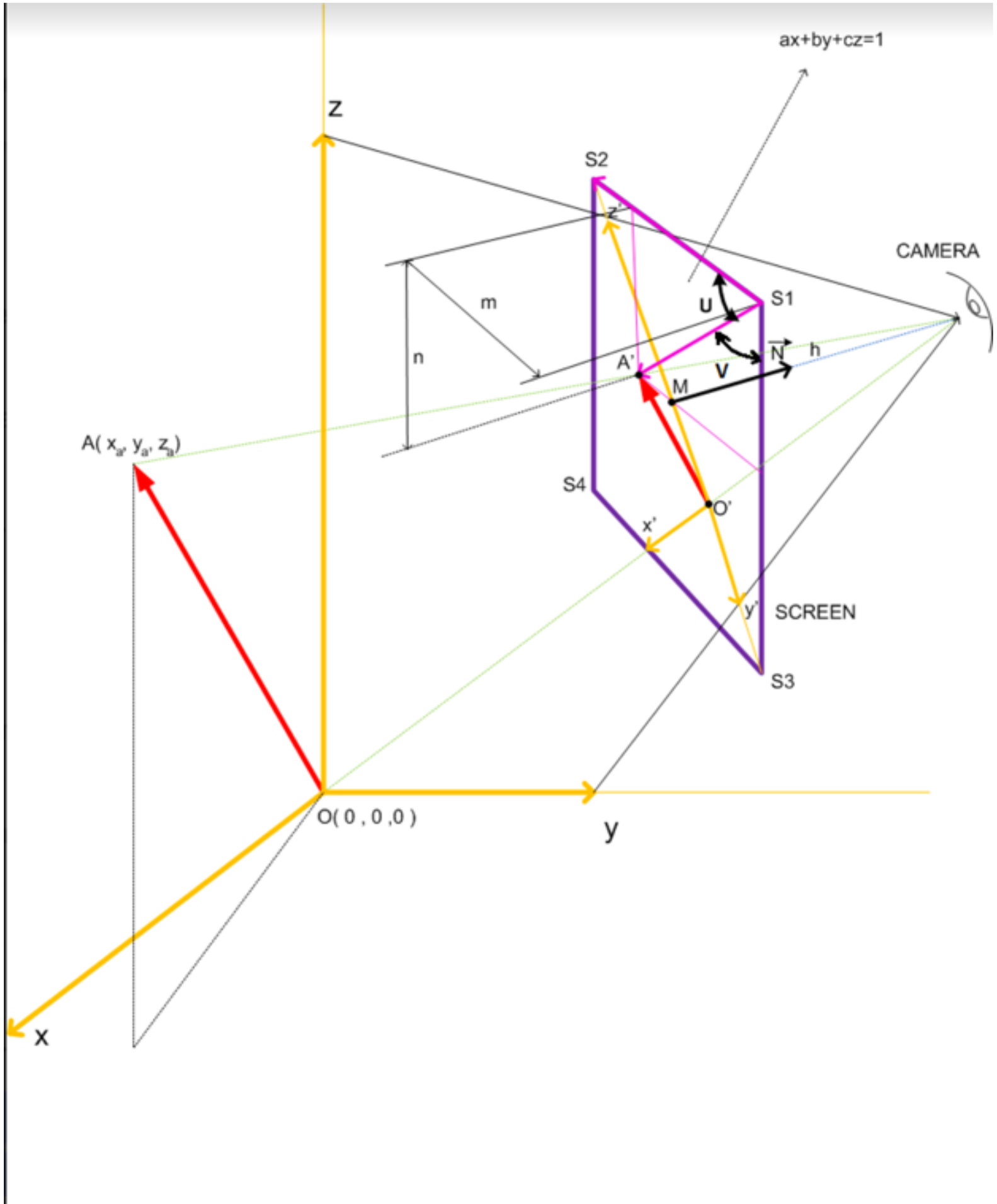
ax+by+cz=1
Z
S2
z'
CAMERA
m
n
U
S1
N
h
A'
V
M
A(x_a, y_a, z_a)
S4
O'
x'
y'
SCREEN
S3
O(0 , 0 ,0)
y
x

What not to do

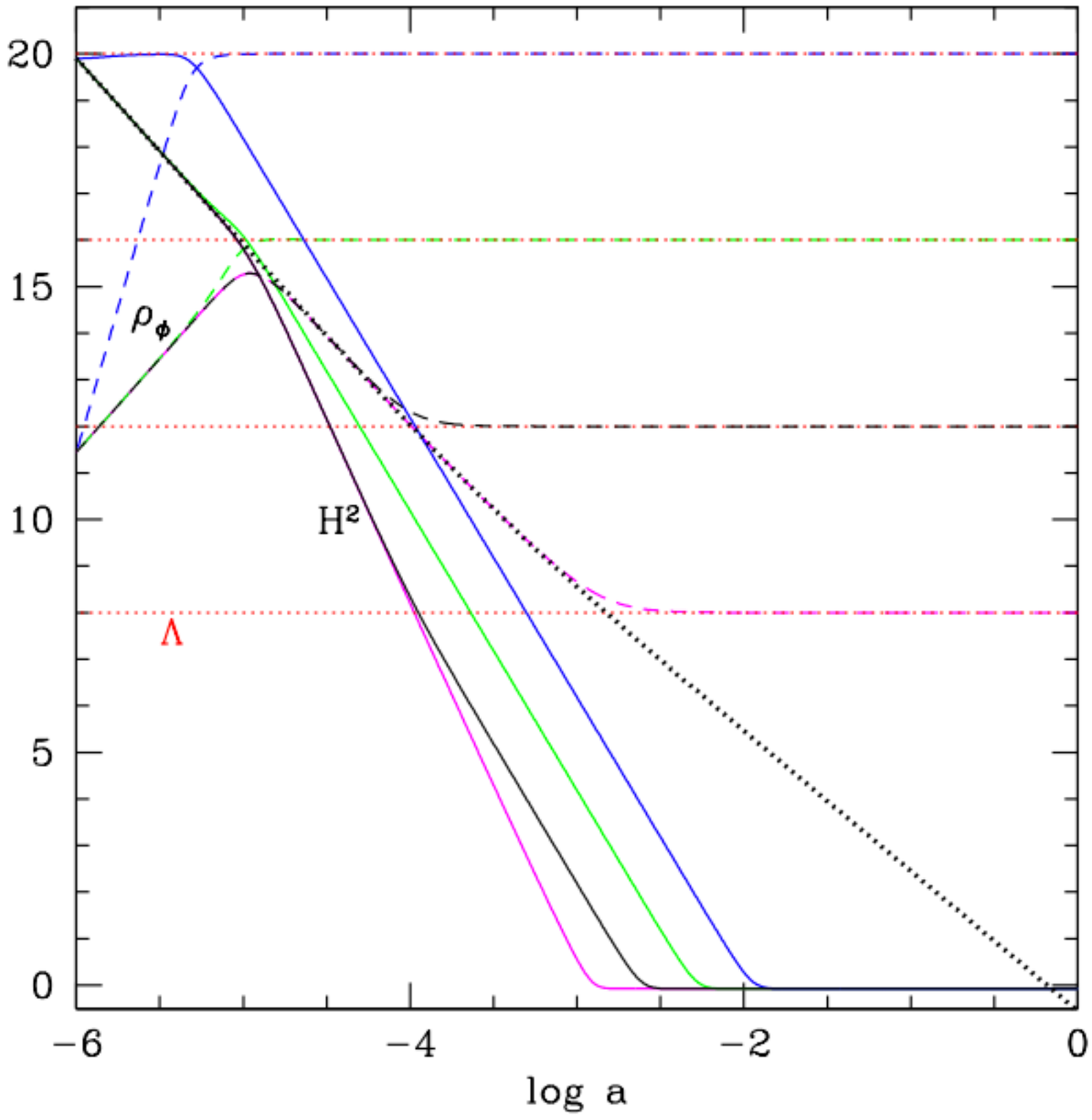

What not to do

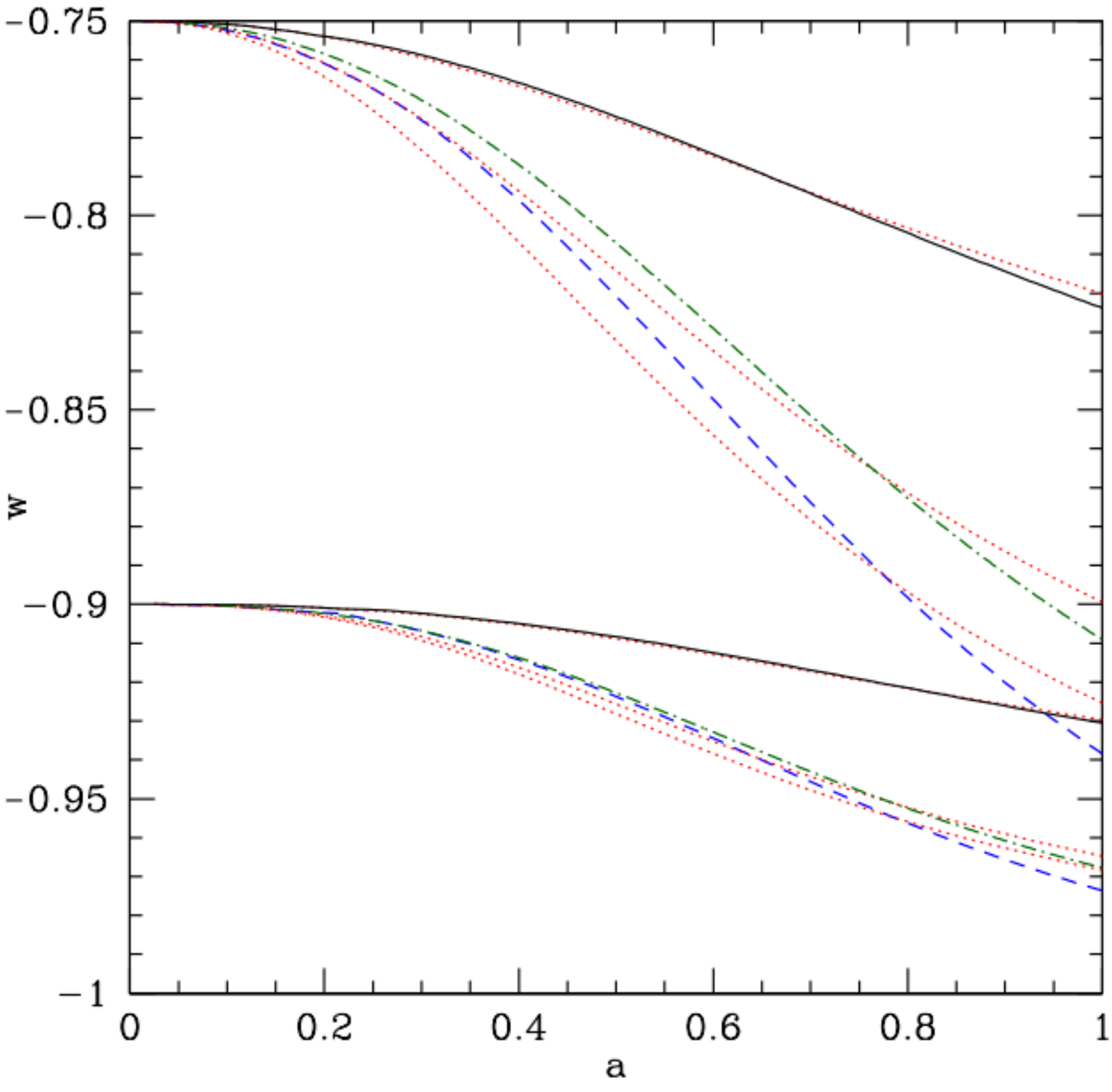

What not to do

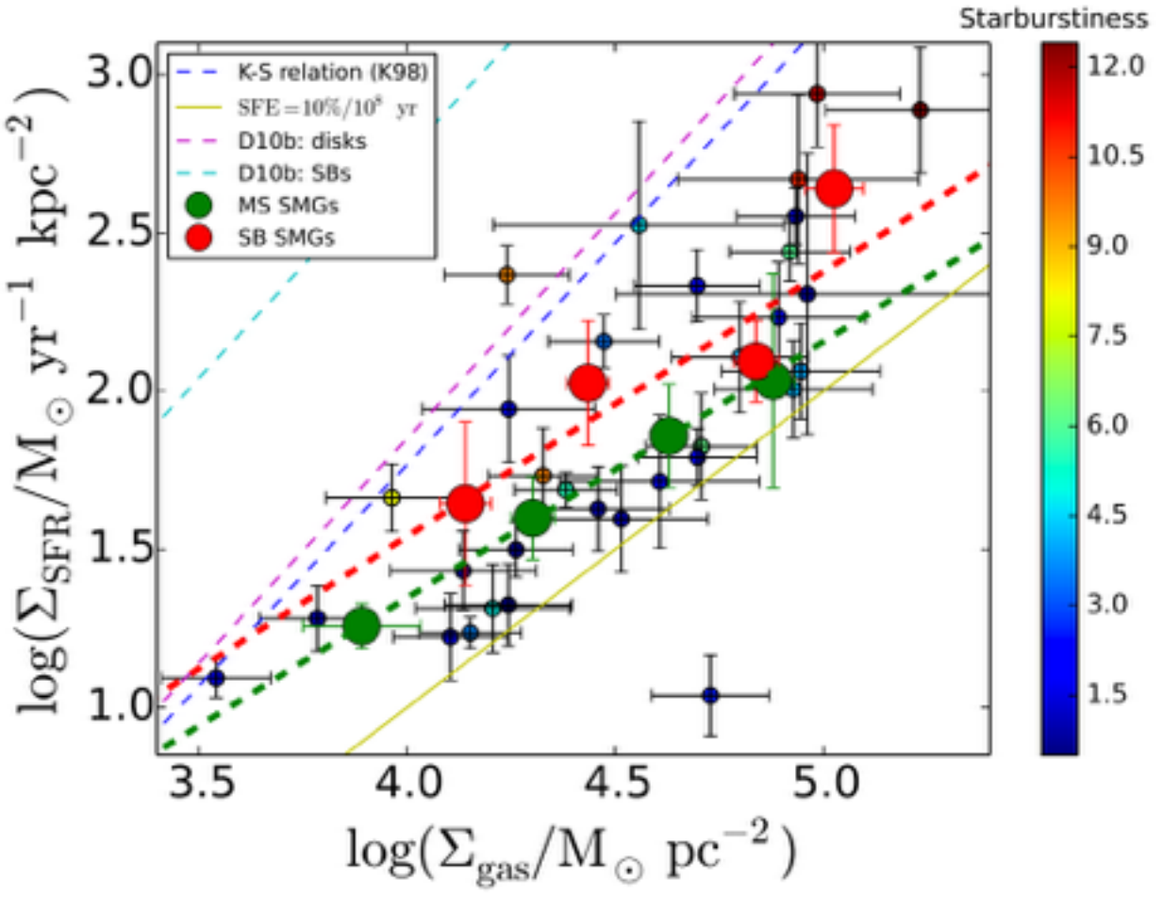

What not to do

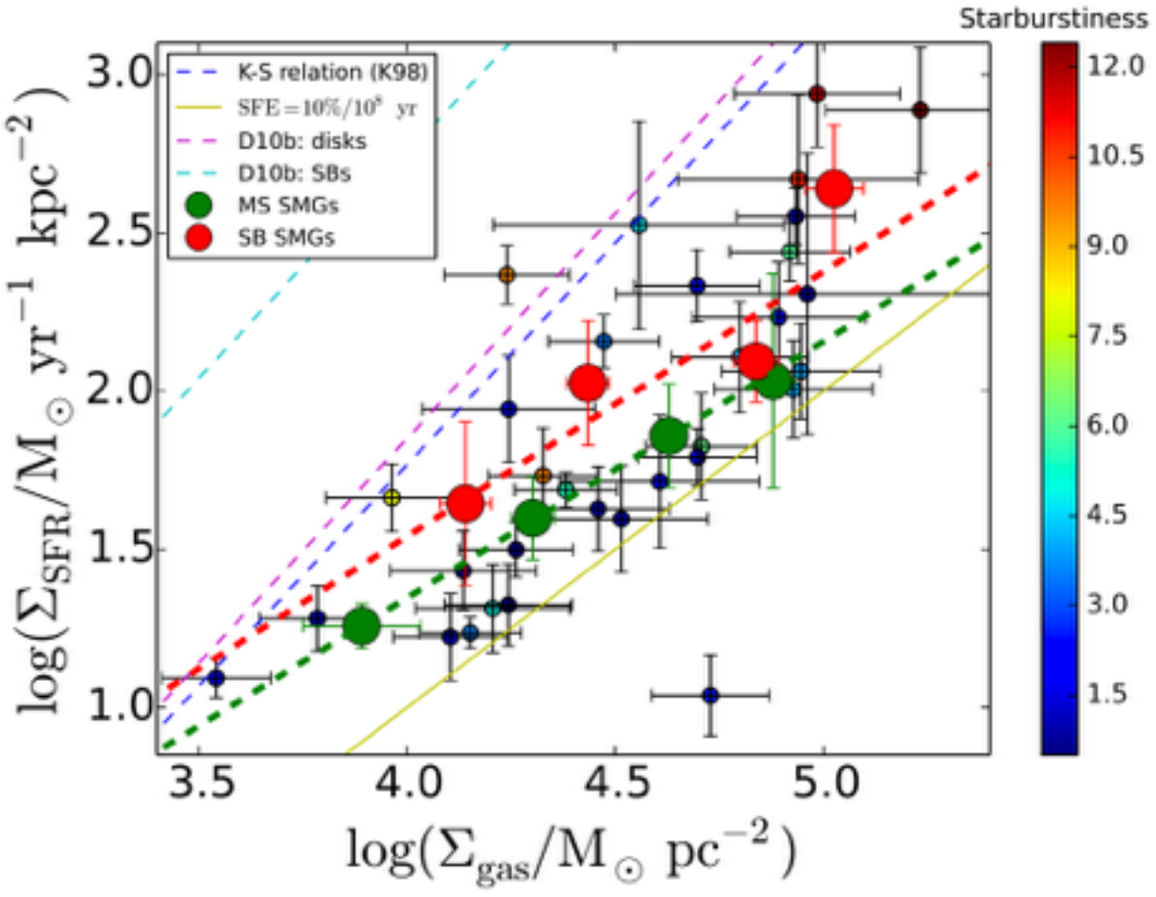

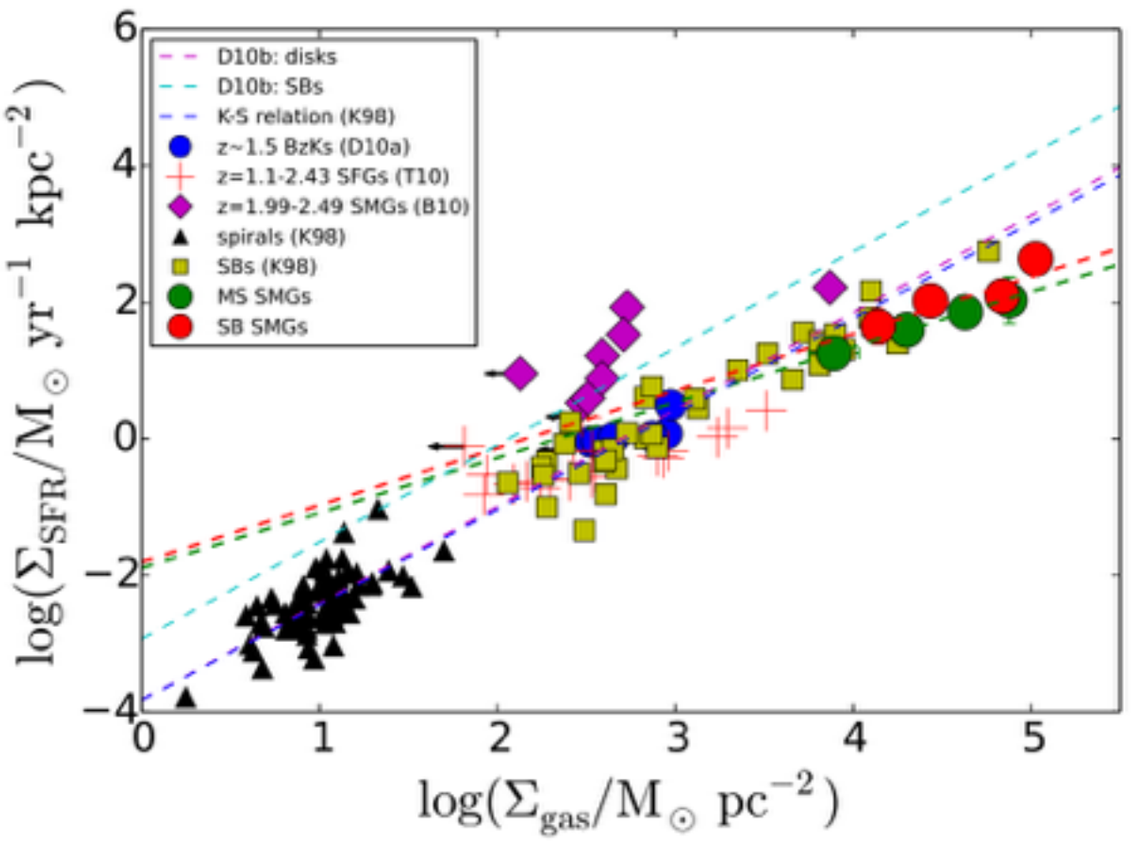

Data

Relationships

Dimensions

Structure

Task:

In pairs, scrape a data set off the internet that you think has a great deal of complexity (decide together why you chose the data).
Split off from each other and make independent plots of the dataset